

**SUPERCONDUCTIVITY AND MAGNETISM
IN LADDER AND CHAIN COMPOUNDS
- PHYSICS OF $(\text{Sr,Ca})_{14}\text{Cu}_{24}\text{O}_{41}$ -**

M. Uehara¹, N. Motoyama², M. Matsuda³, H. Eisaki⁴ and J. Akimitsu²

¹Yokohama National University, Faculty of Engineering, Division of Intelligent Systems Engineering, 79-1 Tokiwadai, Hodogaya-ku, Yokohama, Kanagawa 240-8501, Japan

²Department of Physics and Mathematics, Aoyama-Gakuin University, 5-10-1 Fuchinobe, Sagamihara, Kanagawa 229-8558, Japan

³Advanced Science Research Center, Japan Atomic Energy Research Institute, Tokai, Ibaraki 319-1195, Japan

⁴Nanoelectronic Research Institute, AIST, Tsukuba, Ibaraki 305-8568, Japan

1. INTRODUCTION

The study of ladder materials has in recent years become one of the central issues in the field of condensed matter physics. Ladder materials, which contain a structural unit composed of coupled arrays of one-dimensional (1D) chains, are considered to be an interesting intermediate step between one- and two-dimensional (2D) systems [1-5]. In fact, it is now recognized that the crossover from 1D to 2D is far from straightforward and that ladder materials by themselves exhibit a variety of new physics.

Historically, studies on ladder material were motivated by the discovery of high-transition-temperature (high- T_c) superconductors occurring in 2D spin-1/2 ($S=1/2$) Heisenberg antiferromagnets [6]. Two theoretical predictions have particularly triggered extensive research [1,2].

First, ladders made from an even number of spin-1/2 Heisenberg chains (even-leg ladders) are expected to have a unique spin-liquid ground state with short range spin correlation, where there exists a finite energy gap ("spin gap") to the lowest excited state. The spin gap,

more frequently called the pseudogap, is a key feature of high- T_c superconductors, particularly in the low carrier concentration region. Ladder materials are in this context considered to be good references to gain insights into the pseudogap physics of high- T_c superconductors.

Second, and a more intriguing hypothesis, is the possible occurrence of superconductivity in even-leg ladders when they are doped with holes, similar to the high- T_c materials in which holes are doped into 2D copper-oxygen (CuO_2) planes. The symmetry of pairing is predicted to be d -wave like [7], adding to the similarities between doped ladders and doped 2D planes.

Stimulated by these theoretical suggestions, intensive experimental studies have been carried out, with a variety of cuprate ladder materials having been newly discovered. For instance, (i) the existence of a spin gap was confirmed for SrCu_2O_3 , a prototype of a two-ladder compound [8,9], (ii) hole-doping into two-legged ladders was first achieved on $\text{LaCuO}_{2.5}$ by replacing La with Sr [10], and (iii) superconductivity at 12.5 K was observed in $\text{Sr}_{14-x}\text{Ca}_x\text{Cu}_{24}\text{O}_{41}$ under a pressure of 3 GPa [11].

Here, we review experimental results on cuprate spin ladder materials, emphasizing those for $\text{Sr}_{14-x}\text{Ca}_x\text{Cu}_{24}\text{O}_{41}$. In Sec. 1.2, brief theoretical background is provided, while Sec. 1.3 introduces typical cuprate spin ladder materials. In Chap. 2, we review the magnetic properties of hole-doped edge-sharing $S=1/2$ chains, a constituent of $(\text{Sr,Ca})_{14}\text{Cu}_{24}\text{O}_{41}$, after which the normal state properties of $(\text{Sr,Ca})_{14}\text{Cu}_{24}\text{O}_{41}$ are considered in Chap. 3, with emphasis on the effect of Ca substitution on charge dynamics of hole-doped two-leg ladders. Superconducting properties are then discussed in Chap. 4, being followed by Chap. 5 which discusses the consistency between theory and experiments of ladder and summarizes novel physical insights obtained by a series of experiments on $(\text{Sr,Ca})_{14}\text{Cu}_{24}\text{O}_{41}$. Readers should note that our review is in addition to other excellent reviews on spin ladder system [3-5].

1.2 Theoretical Background

1.2.1 Magnetic ground state of $S=1/2$ ladders

The $S=1/2$ Heisenberg antiferromagnetic (AF) ladders are defined by the Hamiltonian

$$H = J \sum_i S_i \cdot S_{i+\bar{x}} + J' \sum_i S_i \cdot S_{i+\bar{y}}.$$

Here i indicates lattice sites where spin-1/2 operators S_i are located, while J and J' are the AF exchange coupling constant (>0) along the leg and rung of the ladders, respectively (Fig. 1-1(a) and (b)). The width of the ladder depends on the number of legs, with the 1D chain and 2D plane respectively corresponding to one-leg and n -leg ladders having isotropic coupling $J=J'$. Note that 1D and 2D $S=1/2$ AF spin systems are both well understood. In 2D ones, the ground state is a long-range AF order, while in 1D ones the ground state is a “quasi” long-range AF order since a true long-range order is prevented due to a strong quantum fluctuation. In the 1D chain and 2D plane there is no cost in energy to create an excited state with $S=1$, i.e., there is no spin gap.

In contrast to these two limiting cases, spin ladders with an even number of legs behave quite differently, in that the ground state is characterized by a short-range spin correlation. They are accordingly referred to as a “spin-liquid,” having a finite spin gap in their spin excitation spectrum. An intuitive explanation is that J' is much stronger than J (strong

coupling limit), i.e., two neighboring spins located on the same rung form a spin-singlet. The ground state corresponds to the direct product of these spin singlets (Fig. 1-1 (a)). Since each singlet has zero spin, the total spin of the system is zero. To create an excited state, a singlet is turned into a $S=1$ triplet, where one spin triplet has energy J' above the spin singlet. $S=1$ spin excitation propagating along the ladders is represented as the following dispersion

$$E(k) = J' + J \cos(k) .$$

This excitation spectrum apparently has a finite spin gap $\Delta_{SG} = E(\pi) = J' - J$. Although the above description assumes $J \ll J'$, many theoretical studies have confirmed that the essential physics holds down to the other limit of $J' \ll J$, providing J' is finite. In the isotropic ($J=J'$) case, numerical studies estimate Δ_{SG} to be $1/2 \cdot J$ [12,13]. Δ_{SG} decreases with the number of legs, n , which should be expected since the system approaches a gapless 2D plane with increasing n . However, Δ_{SG} is predicted to be finite as long as n takes an even and finite value [2].

Odd-leg ladders show different behavior, i.e., in the strong coupling limit the ground state of the spins located in the same rung has a total spin $1/2$ (Fig. 1-1(b)). The system is therefore considered to be composed of $S=1/2$ 1D AF chains with coupling constant J which is gapless.

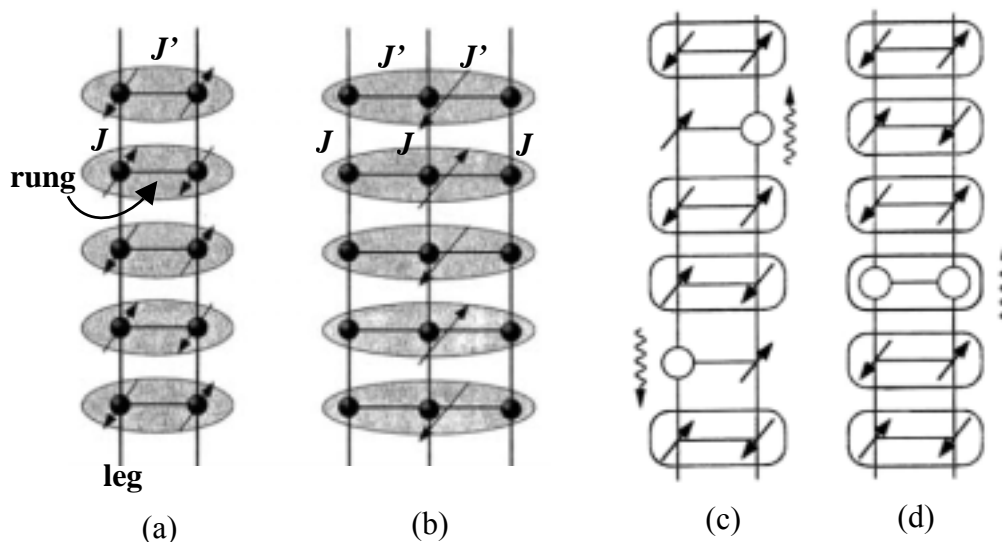


Fig. 1-1

Schematic representations of spin ladders. The ground state of a two- (a) and three- (b) leg ladder in the $J' \gg J$ limit. Pairs of spins along the same rung form a $S=0$ (a) and $S=1/2$ (b) state, respectively. (c) and (d) represent a two-leg ladders doped with two holes. When the holes are located in different rungs, each hole destroys one spin singlet. On the other hand, when two holes reside in the same rung, there is no broken singlet bond (figures from ref. [14]).

1.2.2 Hole-doping into spin ladders

When holes are doped into spin ladders they are expected to interact with the magnetic background. Again, let us consider the strong coupling limit case. When one hole is doped into a two-leg ladder it breaks up one spin singlet bond (Fig. 1-1 (c)) such that the system loses the energy gain caused by the singlet formation. If the second hole is located away from the first one, two singlet pairs are broken. On the other hand, if the two holes are located on the same rung, the number of the broken singlet bond is reduced from two to one. It is therefore energetically more favorable to create a hole pair in the same rung versus creating free spins in a different rung.

Superconductivity in doped ladders is expected to be *d*-wave like in a sense that the pairing amplitude along the legs has a sign opposite from that along the rungs. This is reminiscent of the *d*-wave nature of high- T_c superconductors, presumably suggesting a common origin of superconductivity in two-leg ladders and 2D planes.

Although hole pairing in two-leg ladders may persist as long as a spin gap exists, the spin gap ground state becomes unstable due to hole-doping. In fact, theoretical studies suggest that the magnitude of the spin gap decreases as hole-doping increases [1].

Finally, by making use of gapful spin modes which coexist with gapless ones, Kimura *et al.* [15] reported that superconductivity also appears in three-leg ladders.

1.3 Materials Overview

1.3.1 SrCu_2O_3 and $\text{Sr}_2\text{Cu}_3\text{O}_5$: prototypical two- and three-leg ladders

SrCu_2O_3 and $\text{Sr}_2\text{Cu}_3\text{O}_5$ were discovered by Hiroi *et al.* in 1991 [9], belonging to homologous series $\text{Sr}_{n-1}\text{Cu}_{n+1}\text{O}_{2n}$ ($n = 3, 5, \dots$) composed of $\text{Cu}_{n+1}\text{O}_{2n}$ planes alternating with Sr_{n-1} planes. Figure 1-2 shows the structure of the Cu_2O_3 (Fig. 1-2(a)) and Cu_3O_5 (Fig. 1-2(b)) planes.

The indicated spin ladder structures are formed by introducing a parallel array of planar defects into 2D CuO_2 planes. A Cu^{2+} ion has a single hole in the $d_{x^2-y^2}$ orbital which points toward the oxygen atoms located at the corners of a CuO_4 square. Consequently, within the legs and also along the rungs, a strong superexchange interaction should occur through linear Cu-O-Cu bonds, while the interaction through 90° Cu-O-Cu bonds across the interface between ladders must be much weaker and could even be ferromagnetic. The inter-ladder interactions are also strongly frustrated due to geometrical considerations. Each ladder is nearly isolated as a result.

Magnetic susceptibility ($\chi(T)$), NMR, and μSR measurements of SrCu_2O_3 and $\text{Sr}_2\text{Cu}_3\text{O}_5$ have confirmed the predicted even-odd discrepancy between two- and three-leg ladders [8, 16, 17]. For SrCu_2O_3 , the signature of a spin gap manifests itself as an exponential drop in $\chi(T)$. A fit using $\chi(T) \sim T^{-1/2} \exp(-\Delta_{\text{SG}}/T)$ [18] yields $\Delta_{\text{SG}} = 420$ K [8], while $\Delta_{\text{SG}} = 680$ K is obtained from NMR results [16]. On the other hand, the magnetic ground state of $\text{Sr}_2\text{Cu}_3\text{O}_5$ is a long-ranged AF ordered state with Néel temperature $T_N = 52$ K [17].

Finally, these two systems can only be synthesized under high pressure which makes single crystal growth difficult, and carrier doping has not been successful on either system.

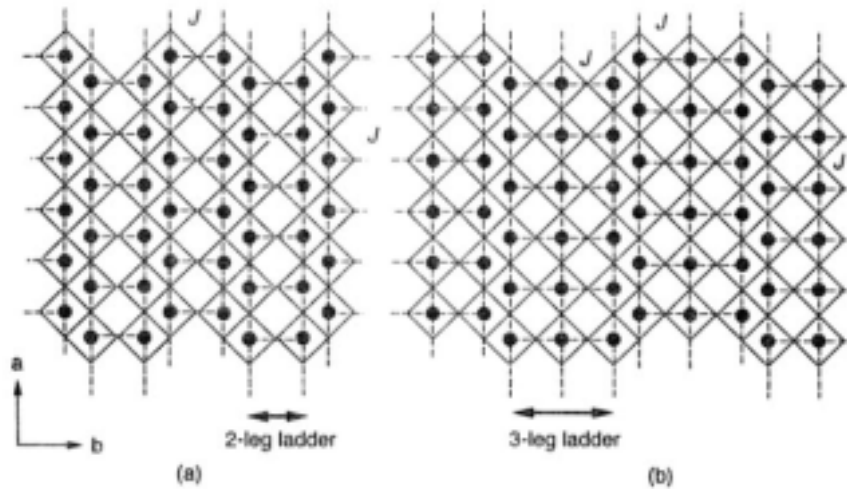


Fig. 1-2

Schematic drawings of the Cu_2O_3 plane of SrCu_2O_3 and Cu_3O_5 plane of $\text{Sr}_2\text{Cu}_3\text{O}_5$. The filled circles are Cu atoms and O atoms are located at the intersection of the solid lines [8].

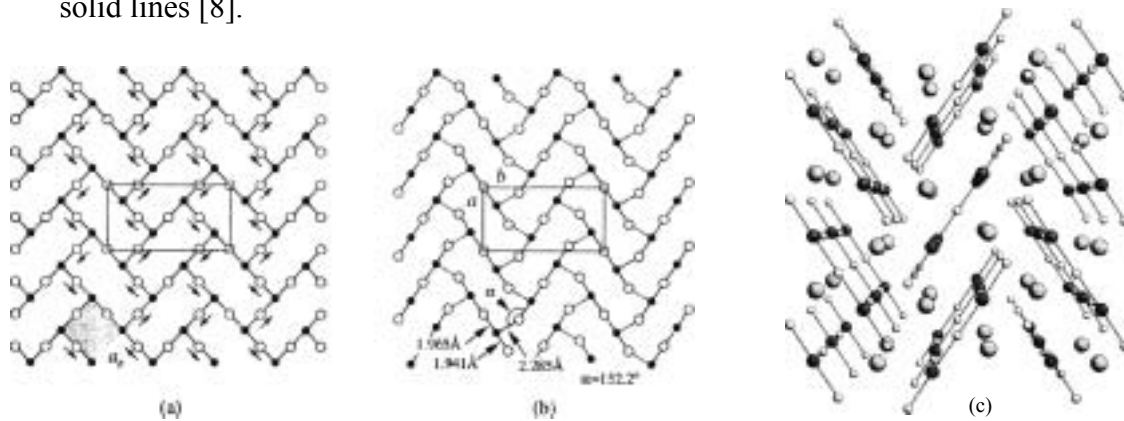


Fig 1-3

Schematic representation of CuO_2 planes in $\text{LaCuO}_{2.5}$. In $\text{LaCuO}_{2.5}$, one of the four oxygen atoms is missing (a). Jahn-Teller distortion forces the displacement of oxygen atoms as indicated by the arrows, resulting in the formation of two-leg ladder structures as shown in (b). In this figure, shorter (longer) Cu-O bonds are shown with solid (broken) lines. (c) Perspective view of $\text{LaCuO}_{2.5}$ along the c -axis. Components of each ladder unit are connected by solid lines. Large, medium, and small balls represent La, Cu, and O atoms, respectively [14].

1.3.2 $\text{LaCuO}_{2.5}$: a hole-doped ladder system

In 1995, Hiroi and Takano [10] succeeded in synthesizing $\text{LaCuO}_{2.5}$ using a high-pressure synthesis technique. This compound contains two-leg ladders within a 3D crystal structure. The framework of $\text{LaCuO}_{2.5}$ is deduced from the LaCuO_3 lattice by creating oxygen vacancies in the basal plane of the CuO_6 octahedra. Rows of oxygen atoms are eliminated along c -axis, thus forming 1D tunnels parallel to this direction. The 1D arrays of oxygen

vacancies, together with the displacement of oxygen atoms due to a Jahn-Teller distortion, create two-leg ladder structures running along the c -axis.

Similar to 2D high- T_c cuprates such as $\text{La}_{2-x}\text{Sr}_x\text{CuO}_4$, one can dope holes into $\text{LaCuO}_{2.5}$ by substituting Sr for La ($\text{La}_{1-x}\text{Sr}_x\text{CuO}_{2.5}$). Resistivity measurements indicate that the insulator-to-metal transition takes place between $x = 0.18$ and $x = 0.20$ [10]. However, contradictory to theoretical conjectures, there is no signature of superconductivity in the metallic sample. Two explanations have been proposed to account for the absence of superconductivity: (1) superconductivity is suppressed due to the random potential caused by the replacement of Sr by La, and (2) finite interladder coupling may stabilize the 3D Néel ordered state instead of a spin-liquid state expected in an isolated spin ladder. Explanation (2) seems to be consistent with the NMR and μSR results which report the presence of an antiferromagnetic order below $T_N \sim 110$ K in $\text{LaCuO}_{2.5}$ [19, 20].

1.3.3 $\text{A}_{14}\text{Cu}_{24}\text{O}_{41}$ (A=Sr, Ca, Ba, Y, La) : a superconducting ladder

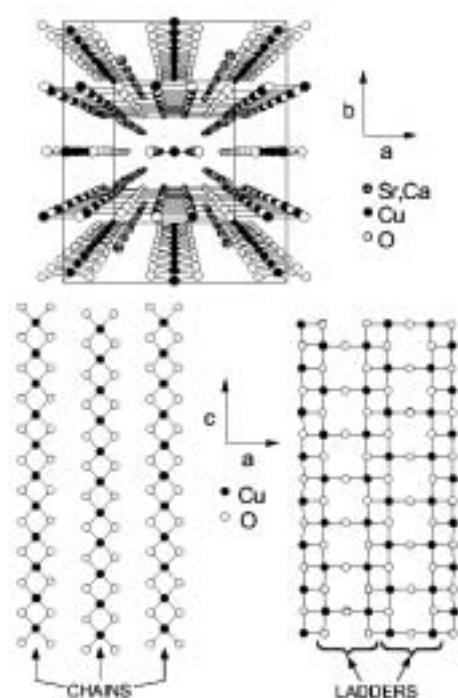


Fig. 1-4 Crystal structure of $(\text{Sr,Ca})_{14}\text{Cu}_{24}\text{O}_{41}$

$\text{A}_{14}\text{Cu}_{24}\text{O}_{41}$, a so called “telephone number” compound, was first reported by McCarron *et al.* and Siegrist *et al.* [21, 22]. It is classified as a composite crystal since it is composed of multiple interpenetrating layered substructures, namely, edge-sharing CuO_2 chain planes, A-planes, and Cu_2O_3 -two-leg ladder planes (Fig. 1-4). The two Cu-O substructures are mutually incommensurate because the ratio of their lattice constants along the c -axis (along the ladders/chains), $c_{\text{ladder}}/c_{\text{chain}}$, takes an irrational value. These two substructures become nearly commensurate at $10 \times c_{\text{chain}} \sim 7 \times c_{\text{ladder}} \sim 27 \text{ \AA}$. Due to mutual incommensurability, structural modulations between the substructures may occur. The a -axis (along the rung) and b -axis (perpendicular to the ladder planes) unit cell lengths are 11.48 and 13.41 \AA , respectively.

Single crystals can be grown by the traveling-solvent floating zone method, and a high O_2 -

gas pressure of 10 atm is needed for high-Ca doping samples.

Physical properties dramatically change by the chemical substitution of Sr atoms. Although the nominal Cu valence of $\text{Sr}_{14}\text{Cu}_{24}\text{O}_{41}$ is +2.25 such that the holes are “self-doped” into the system even in a pristine form, $\text{Sr}_{14}\text{Cu}_{24}\text{O}_{41}$ nevertheless shows insulating behavior. The existence of a spin gap in the Cu_2O_3 -two-leg ladder plane has been confirmed by many experiments [23-28], with metallic behavior being observed through the substitution by Ca in a form $\text{Sr}_{14-x}\text{Ca}_x\text{Cu}_{24}\text{O}_{41}$ with $x > 10$. Superconductivity appears when a high pressure, typically more than 3GPa, is applied to metallic samples.

As described in the following chapters, extensive experimental research on $\text{Sr}_{14-x}\text{Ca}_x\text{Cu}_{24}\text{O}_{41}$ has revealed fundamental physical properties of hole-doped edge-sharing chains and two-leg ladders.

2. MAGNETISM IN THE EDGE-SHARING CuO_2 CHAINS

2.1 Magnetic Properties of the Edge-Sharing CuO_2 Chains for the $\text{Sr}_{14}\text{Cu}_{24}\text{O}_{41}$ -type Compound

2.1.1 Basic properties of the $\text{Sr}_{14}\text{Cu}_{24}\text{O}_{41}$ -type compound

$\text{Sr}_{14}\text{Cu}_{24}\text{O}_{41}$ consists of a Cu_2O_3 -two-leg ladder plane and edge-sharing 1D CuO_2 chain plane. The low-energy magnetic properties exhibited by this compound are determined by those in the 1D chain, i.e., the spins in the Cu_2O_3 ladder form a singlet ground state with a large spin gap $\Delta_{\text{SG}} \sim 40$ meV (described in Chap. 3). This section discusses magnetic properties of the 1D chain of the $\text{Sr}_{14}\text{Cu}_{24}\text{O}_{41}$ -type compound.

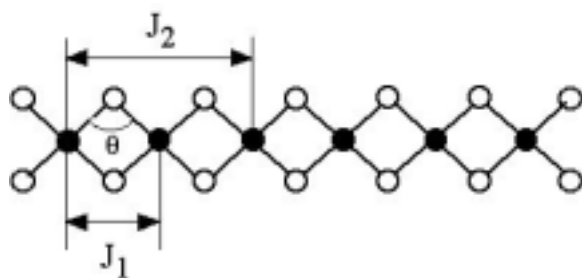


Fig. 2-1 A schematic structure of the edge-sharing 1D CuO_2 chain. Filled and open circles correspond to Cu and O ions, respectively. θ represents the bond angle between Cu and O.

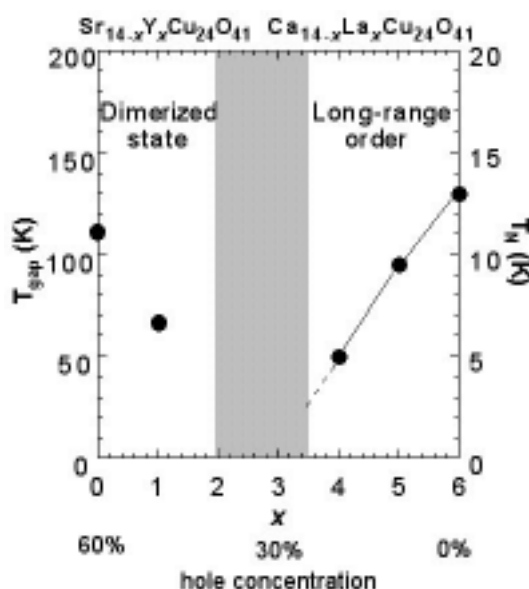


Fig. 2-2 The magnetic phase diagram in $\text{Sr}_{14-x}\text{Y}_x\text{Cu}_{24}\text{O}_{41}$ and $\text{Ca}_{14-x}\text{La}_x\text{Cu}_{24}\text{O}_{41}$ as a function of x or hole concentration.

Figure 2-1 shows a schematic structure of the edge-sharing 1D chain, where copper spins are coupled along the chains by the nearly 90° Cu-O-Cu interaction. The nearest-neighbor (NN) and the next-nearest-neighbor (NNN) exchange interactions are denoted by J_1 and J_2 , respectively. The value of J_1 and J_2 strongly depend on the bond angle θ and bond distance $d_{\text{Cu-O}}$ [29]. In particular, J_1 changes its sign at $\theta = 95^\circ$.

Another interesting feature of the 1D chain in $\text{Sr}_{14}\text{Cu}_{24}\text{O}_{41}$ is that it can be hole-doped. The doped holes, which are located at O $2p$ orbitals, strongly couple with Cu^{2+} ions so as to form

a $S=0$ singlet state (frequently referred to as Zhang-Rice (ZR) singlet) [30]. Hole-doping into the chains is therefore equivalent to introducing a $S=0$ state in the spin chain. For $\text{Sr}_{14}\text{Cu}_{24}\text{O}_{41}$, the number of holes can be controlled by the chemical substitution of trivalent ions such as La^{3+} or Y^{3+} ions at the Sr site in forms of $\text{Sr}_{14-x}\text{Y}_x\text{Cu}_{24}\text{O}_{41}$ and $\text{Ca}_{14-x}\text{La}_x\text{Cu}_{24}\text{O}_{41}$. Figure 2-2 shows a magnetic phase diagram of the substituted system, where the end material $\text{Ca}_8\text{La}_6\text{Cu}_{24}\text{O}_{41}$, in which all Cu atoms in the chains (also in the ladders) are divalent and carry $S=1/2$ spins, exhibits a magnetic order below $T_N = 12.2$ K [31, 32]. The Cu moments are aligned ferromagnetically along the chain (c -axis) such that these ferromagnetic chains form a spiral structure with a rotation angle of $\sim 2\pi/5$ along the a -axis [32]. Along the b -axis, however, the spins are aligned antiferromagnetically. Upon hole-doping, T_N gradually decreases as indicated. $\text{Ca}_9\text{La}_5\text{Cu}_{24}\text{O}_{41}$, in which holes are slightly introduced ($\sim 10\%$), has a long-range AF order below $T_N = 10.5$ K with a commensurate magnetic structure—a ferromagnetic arrangement within the chain and antiferromagnetic correlations between chains [33]. This long-range AF order disappears around $x \sim 3$. For $x < 3$, a dimerized singlet state shows up as a magnetic ground state. The singlet ground state becomes most stable in the end material $\text{Sr}_{14}\text{Cu}_{24}\text{O}_{41}$ with a hole concentration of 60 %.

2.1.2 Singlet ground state in $\text{Sr}_{14}\text{Cu}_{24}\text{O}_{41}$

The singlet ground state in the 1D chain in $\text{Sr}_{14}\text{Cu}_{24}\text{O}_{41}$ was first reported using magnetization [31,34,35] and ESR measurements [35]. Figure 2-3 shows the temperature dependence of the magnetic susceptibility ($\chi(T)$) for $\text{Sr}_{14}\text{Cu}_{24}\text{O}_{41}$, together with those for the Y- and Ca-substituted samples [36]. Note that $\chi(T)$ is dominated by the contribution from the 1D chain since the spins in the Cu_2O_3 ladder form a singlet ground state with a large spin gap $\Delta_{\text{SG}} \sim 40$ meV. As shown in Fig. 2-3 (a), $\chi(T)$ indicates a broad peak and a subsequent drop at low temperatures. This drop is isotropic and goes down to zero after subtracting the Curie term contribution; thereby suggesting the formation of a spin gap with magnitude of about 130 K. Many studies have been performed to elucidate the origin of the spin gap in the 1D chains, making it clear that the nonmagnetic Cu sites (ZR singlets) play an important role. For example, a neutron scattering study revealed that the spin singlet ground state consists of the dimers formed by two $S=1/2$ Cu^{2+} spins and one ZR singlet located between the two Cu^{2+} spins [37]. The exchange interaction between the two Cu spins (~ 10 meV) is mediated via a nonmagnetic ZR singlet. A question arises as to how the dimers are arranged and interact with each other. Although it was first thought that each dimer is separated by one ZR singlet [37], ultimately each dimer was found to be separated by two ZR singlets as described next [24,38,39].

NMR studies have revealed local microscopic properties of the dimerized state [25-27,40,41]. Takigawa *et al.* [40] found NMR signals originating from both magnetic Cu^{2+} and the nonmagnetic ZR singlet in the chain. A NMR peak originating from the ZR singlet gradually splits into two peaks below ~ 200 K with a subsequent splitting below ~ 100 K (Fig. 2-4). The temperature dependence of this shift suggests there are two inequivalent ZR singlet sites; i.e., one is the constituent of the dimer located between two Cu^{2+} spins, while the other ZR singlet would be located between the dimers. NMR results, however, cannot determine spacial arrangement of the dimers and ZR singlets.

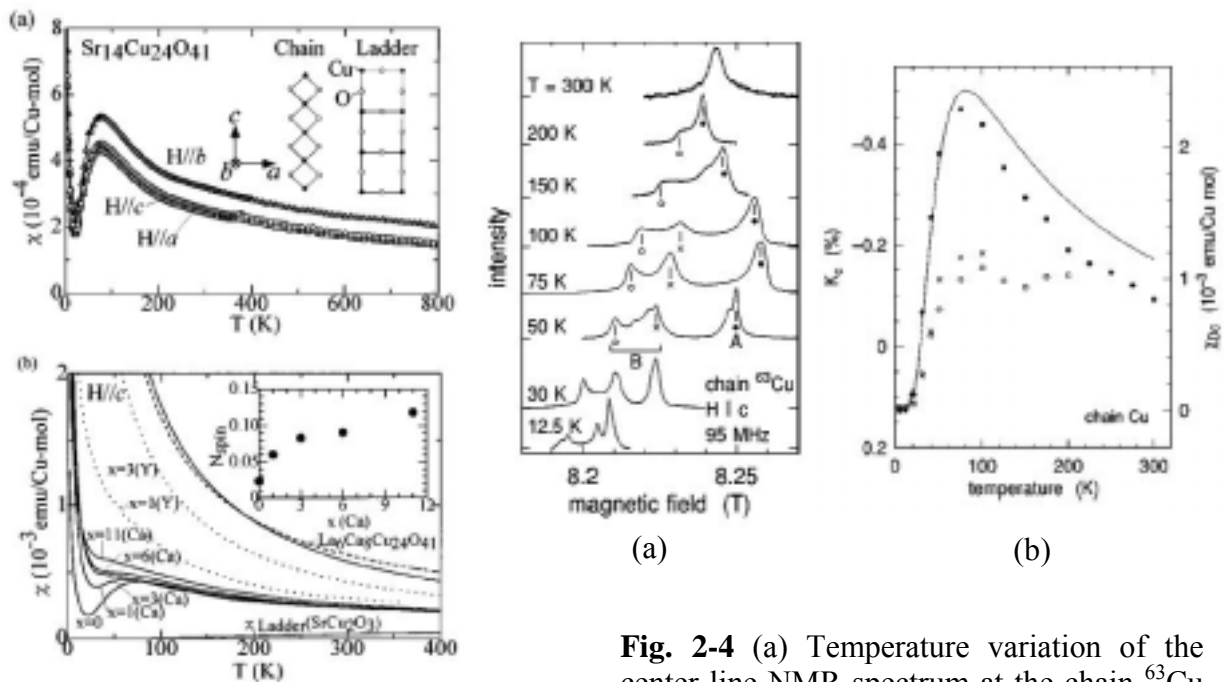


Fig. 2-3 Temperature dependence of the magnetic susceptibility in $\text{Sr}_{14}\text{Cu}_{24}\text{O}_{41}$, $\text{Sr}_{14-x}\text{Ca}_x\text{Cu}_{24}\text{O}_{41}$, $\text{Sr}_{14-x}\text{Y}_x\text{Cu}_{24}\text{O}_{41}$, and $\text{La}_6\text{Ca}_8\text{Cu}_{24}\text{O}_{41}$. [36]

Fig. 2-4 (a) Temperature variation of the center line NMR spectrum at the chain ^{63}Cu sites obtained at 95 MHz for $H//c$ in $\text{Sr}_{14}\text{Cu}_{24}\text{O}_{41}$. (b) Temperature dependence of the shift along the c -direction at the chain ^{63}Cu sites [40].

Based on neutron scattering results, Eccleston *et al.* [24] proposed a model in which each dimer is separated by two ZR singlets such that the magnetic unit cell is five times larger than the structural unit cell. Experimental results are quantitatively reproduced using the AF intradimer coupling constant 11.2 meV and ferromagnetic interdimer coupling -1.1 meV. It should be noted that due to insufficient resolution the two excitation branches expected from their model could not be separated. Finally, Regnault *et al.* [38] and Matsuda *et al.* [39] independently reported measuring two branches over a wide range of Q in the ac plane, originating from weak interchain couplings along both the a and c directions. The study by Matsuda *et al.* [39] is briefly summarized as follows.

Figure 2-5 shows the observed dispersion relation and energy-integrated intensities. In order to analyze the observed data, a model Hamiltonian is employed to describe the dispersion of the dimers which are weakly coupled along the a - and c -axes (Fig. 2-6). It is known that such dimers, namely weakly coupled dimers, can be well described by the Random Phase Approximation (RPA). The coupling constants indicated in Fig. 2-6 are estimated to be $J = 11$ meV, $J_a = 0.75$ meV, and $J_c = 0.75$ meV. In this dispersion relation the averaged excitation energy, band width of each excitation mode, and energy difference between the acoustic and optic modes are related to J , J_c , and J_a , respectively. Figure 2-5 indicates the calculated dispersion relation and energy-integrated intensities corresponding to the acoustic and optic modes, respectively. Experimental results are well described by RPA theory, guaranteeing the validity of the model shown in Fig. 2-6. However, the charge ordering obtained in this analysis has not been observed by either electron diffraction or

synchrotron x-ray measurements, probably because charge ordering is not so long-ranged and static.

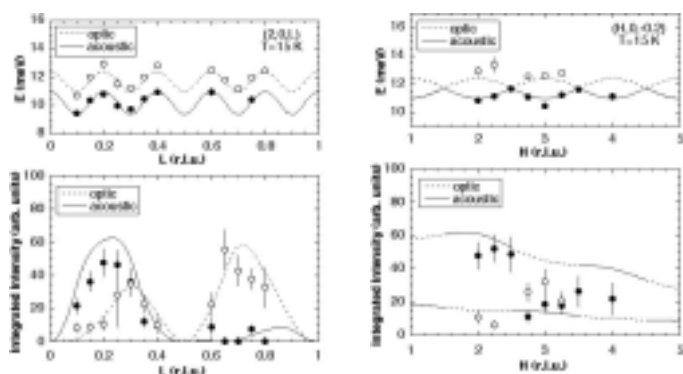


Fig. 2-5 Observed and calculated energies and intensities at $(2,0,L)$ and $(H,0,-0.2)$ measured at 15 K in $\text{Sr}_{14}\text{Cu}_{24}\text{O}_{41}$ [39]. Solid lines indicate the calculated curves.

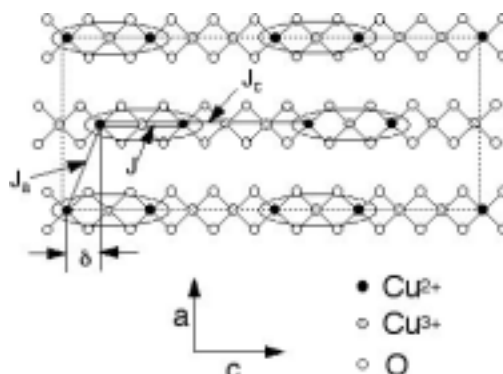


Fig. 2-6 A proposed model for the dimerized state and the ordering of Cu^{2+} and ZR singlet in the ac plane in $\text{Sr}_{14}\text{Cu}_{24}\text{O}_{41}$. [39]

Next we discuss other structural studies on the 1D chains plane for $\text{Sr}_{14}\text{Cu}_{24}\text{O}_{41}$. An electron diffraction study revealed a temperature-independent modulated structure along the chain which originates from the lattice mismatch between the 1D chain layer and Cu_2O_3 ladder layer and depends on oxygen stoichiometry [42]. It was found that more stoichiometric $\text{Sr}_{14}\text{Cu}_{24}\text{O}_{41}$ has a more homogeneous superstructure with a five times larger unit cell along the chain. From synchrotron x-ray studies, a specific structural coupling along the c direction was proposed based on temperature-dependent superlattice reflections, possibly originating from a structural distortion [43,44]. In particular, Fukuda *et al.* [44] reported a structural distortion with five times periodicity. The most comprehensive model was proposed by Gotoh *et al.* [45] based on a single crystal x-ray diffraction study together with a bond valence sum analysis. There is, however, another interpretation for the data, i.e., the additional reflections are due to interactions between the two structure blocks in this composite crystal such that their presence is not related to a possible charge order [46].

2.1.3 Substitution effect

The substitution effect on the singlet dimerized state was also investigated, with the introduction of Y^{3+} for Sr^{2+} resulting in turning the nonmagnetic ZR singlet into $S=1/2 \text{Cu}^{2+}$. As shown in Fig. 2-3, Y substitution increases the Curie term contribution and reduces the magnitude of the spin gap [47]. Neutron scattering studies have shown that Y substitution broadens the magnetic excitation peaks and reduces the gap energy while preserving the periodicity of the dimer arrangement [37,48]. The isovalent Ca^{2+} substitution for Sr^{2+} is also known to gradually reduce the number of the holes in the chain because some amount of holes in the chains are transferred to the ladder layers by Ca substitution as explained in Chap. 3 [49]. Ca substitution subsequently affects the dimerized state in the chain similar to Y substitution, although its effect is weaker. NMR and magnetic susceptibility measurements showed that the gap energy does not change drastically with Ca substitution [26,31,34], while

neutron scattering measurements in $\text{Sr}_{11}\text{Ca}_3\text{Cu}_{24}\text{O}_{41}$ showed that coupling constants J , J_c , and J_a and the periodicity of the dimer arrangement are nearly identical compared to the non-substituted $\text{Sr}_{14}\text{Cu}_{24}\text{O}_{41}$, although the dimerized state becomes unstable [39]. These results indicate that hole order sensitively depends on the hole concentration as well as disorder, and that long-range dimer formation is disturbed by Y or Ca substitution.

2.1.4 Magnetic interactions in the AF phase

The magnetic properties of the AF ordered phase were studied in $\text{Ca}_{14-x}\text{La}_x\text{Cu}_{24}\text{O}_{41}$. Based on magnetization, heat capacity, [50] and ESR measurements [51], we know that $\text{Ca}_9\text{La}_5\text{Cu}_{24}\text{O}_{41}$ has an Ising-like anisotropy which is unusual for Cu oxides having spin-orbit coupling that is believed to be negligibly small.

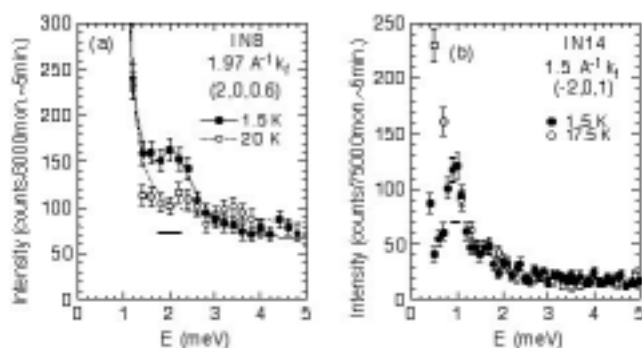


Fig. 2-7 Typical inelastic neutron spectra observed at $(H,0,L)$ below and above T_N for the edge-sharing 1D chain in $\text{Ca}_9\text{La}_5\text{Cu}_{24}\text{O}_{41}$. The lines are guides to the eyes. The horizontal bars represent the instrumental energy resolution [54].

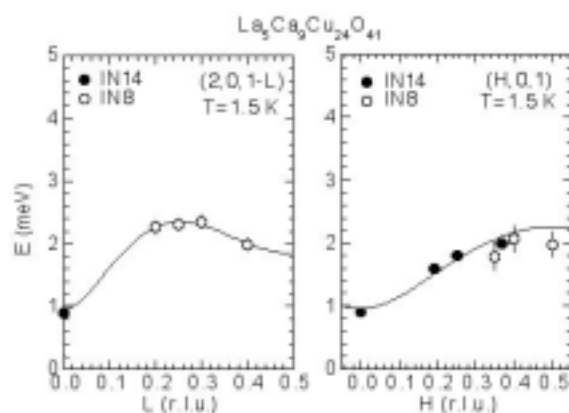


Fig. 2-8 ω - Q dispersion relation along and perpendicular to the c -axis for the edge-sharing 1D chain in $\text{Ca}_9\text{La}_5\text{Cu}_{24}\text{O}_{41}$ [54].

The origin of large spin-orbit coupling, giving rise to anisotropic exchange interactions, was theoretically studied by Yushankhai and Hayn [52] and Tornow *et al.* [53]. Inelastic neutron scattering measurements have also been performed on the AF phase of $\text{Ca}_9\text{La}_5\text{Cu}_{24}\text{O}_{41}$ [54]. Figure 2-7 shows typical inelastic neutron spectra observed at $(H,0,L)$, where the peak width in energy is broader than the instrumental resolution even around the zone center. It is remarkable that broadened excitations are observed even when the magnetic order is static and long-ranged. The excitation peak also becomes broader with increasing Q both parallel and perpendicular to the chain. To analyze the observed dispersion relation (Fig. 2-8), linear-spin-wave theory including uniaxial anisotropy was applied by introducing into the calculation exchange coupling constants between two spins (Fig. 2-9). The solid curve in Fig. 2-8 represents the result of a fit with $J_{c1} = 0.20(7)$ meV, $J_{c2} = -0.18(5)$ meV, $J_{ac1} = 2 J_{ac2} = 0.681(1)$ meV, and $D = -0.211(1)$ meV, where D represents an effective uniaxial anisotropic interaction [54]. Calculated values reproduce experimental results reasonably well. The excitation gap at the zone center is due to uniaxial anisotropy along the b -axis originating

from an anisotropic exchange interaction. The antiferromagnetic ($J_{c1} > 0$) NN and ferromagnetic ($J_{c2} < 0$) NNN interactions obtained from the neutron scattering data may prefer an antiferromagnetic order in the chain although the actual magnetic arrangement is ferromagnetic.

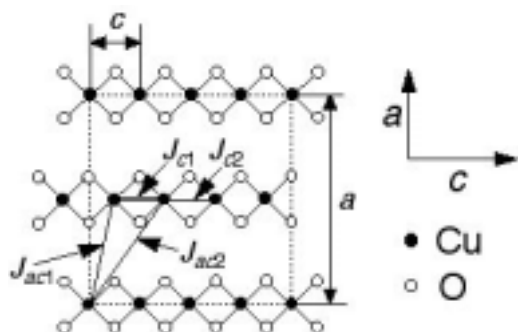


Fig. 2-9 Structure of the edge-sharing 1D chains in the ac plane in $\text{Ca}_9\text{La}_5\text{Cu}_{24}\text{O}_{41}$. Below $T_N=10.5$ K the Cu^{2+} spins align ferromagnetically along the chain (c -axis) with the propagation vector $k = [110]$. The spins point along the b -axis [54].

On the other hand, antiferromagnetic inter-chain couplings J_{ac1} and J_{ac2} are comparable to J_{c1} and have a number of bonds equal to twice that of J_{c1} (Fig. 2-9). Although there exist competing interactions between intra-chain couplings (J_{c1} and J_{c2}) and inter-chain couplings (J_{ac1} and J_{ac2}), the latter is dominant such that the magnetic arrangement in the chain becomes ferromagnetic. It should be noted that the end material $\text{Ca}_8\text{La}_6\text{Cu}_{24}\text{O}_{41}$ shows an incommensurate magnetic structure perpendicular to the chain (a -axis) with a ferromagnetic arrangement along the chain (c -axis) [32]. This observed incommensurate structure is possibly a consequence of a delicate balance of frustrating interactions between intra- and inter-chain interactions.

This neutron scattering study additionally showed that the uniaxial anisotropic interaction D is comparable with the small isotropic interactions both parallel and perpendicular to the chain, being unexpected based on the geometrical structure and giving rise to an enhancement of the Ising-like anisotropy. The small exchange interactions suggest that the bond angle between copper and oxygen ions is close to 95° [29]. Since spin-wave excitations were also broadened considerably, the broadening is probably enhanced by frustrating interactions between intra- and inter-chain interactions, and by disorder due to a structural distortion and doped holes. Such behavior is also unexpected based on the simple geometrical structure.

A theoretical study showed that when the above simple model is based on semi-classical spin-wave theory, it is insufficient to describe the magnetic transition temperature and results of magnetization measurements [55], which suggests that some formation of the charge order should be taken into account to fully understand the system's magnetic properties [56, 57].

Another interesting feature of this system is that magnetic moments can be induced at oxygen sites due to strong Cu d -O p hybridization. Weht and Pickett [58] theoretically predicted that large moments ($\sim 0.2 \mu_B$) lie on the oxygen ions in the CuO_2 chains in Li_2CuO_2 . Finally, in the edge-sharing 1D chain of $\text{Ca}_9\text{La}_5\text{Cu}_{24}\text{O}_{41}$ it was observed that magnetic moments exist at oxygen sites ($\sim 0.02 \mu_B$) as well as at Cu sites ($\sim 0.2 \mu_B$) [33]. Oxygen moments were also observed in related compounds $\text{Ca}_2\text{Y}_2\text{Cu}_5\text{O}_{10}$ [59] and Li_2CuO_2 [60,61].

2.2 Magnetic Properties in a Related Compound $\text{Ca}_{2+x}\text{Y}_{2-x}\text{Cu}_5\text{O}_{10}$

The $\text{Ca}_{2+x}\text{Y}_{2-x}\text{Cu}_5\text{O}_{10}$ system [62-64] consists of edge-sharing CuO_2 chains which are nearly the same as those in $\text{Ca}_{14-x}\text{La}_x\text{Cu}_{24}\text{O}_{41}$. Since the system does not have Cu_2O_3 ladder

planes, it is a good candidate to study the hole-doping effect on the magnetic ground state and excitations purely in the chain. Figure 2-10 shows the structure of the edge-sharing CuO_2 chains in $\text{Ca}_{2+x}\text{Y}_{2-x}\text{Cu}_5\text{O}_{10}$. Hayashi *et al.* [64] reported that this system remains insulating even when holes are doped by 40%.

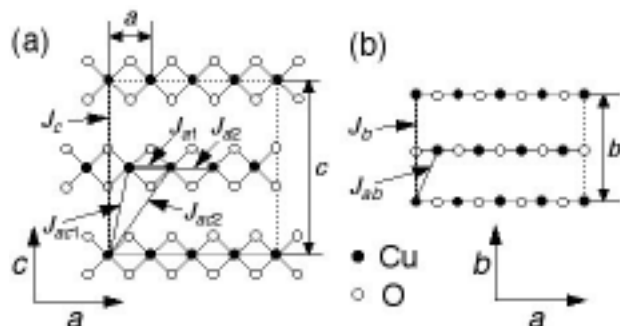


Fig. 2-10 Structure of edge-sharing CuO_2 chains in the ac plane in $\text{Ca}_2\text{Y}_2\text{Cu}_5\text{O}_{10}$. Oxygen ions are located at $z \sim \pm 0.125$ in (b). Below $T_N = 29.5$ K the Cu^{2+} spins align ferromagnetically along the chain (a -axis) with the propagation vector $k = [001]$ [74].

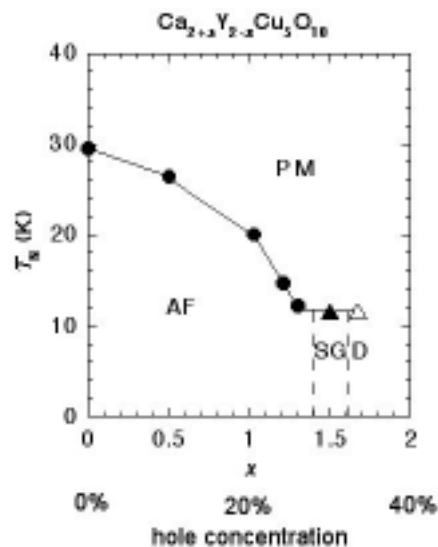


Fig. 2-11 The magnetic phase diagram in $\text{Ca}_{2+x}\text{Y}_{2-x}\text{Cu}_5\text{O}_{10}$ as a function of x and hole concentration. The open triangle shows that the magnetic state is minor. PM, AF, SG, and D indicate paramagnetic, antiferromagnetic, spin-glass, and nearly disordered phases, respectively [76].

Figure 2-11 shows the magnetic phase diagram of the $\text{Ca}_{2+x}\text{Y}_{2-x}\text{Cu}_5\text{O}_{10}$ system, where the end-material $\text{Ca}_2\text{Y}_2\text{Cu}_5\text{O}_{10}$, which has no holes, indicates AF order of the Cu^{2+} moment below $T_N = 29.5$ K with ferromagnetic coupling along the chain [65,66]. Note the magnetic structure in the CuO_2 plane (ac plane) is the same as that in $\text{Ca}_{14-x}\text{La}_x\text{Cu}_{24}\text{O}_{41}$. The ordered moment of Cu^{2+} is $\sim 0.9 \mu_B$ at low temperatures, being comparable to the full magnetic moment of the free Cu^{2+} ion. The long-range AF order is suppressed by hole-doping and is replaced by a spin-glass behavior above $x = 1$. In the spin-glass region ($x \sim 1.5$), magnetic susceptibility measurements show a difference between field-cooling and zero-field-cooling processes [67]. In the $x = 1.5$ crystal, a neutron scattering study showed a broad transition to short-range ordered magnetic phase below ~ 15 K. The magnetic correlation lengths are $\xi_a \sim 28$ Å, $\xi_b \sim 12$ Å, and $\xi_c \sim 2$ Å at low temperature. In the $x = 1.67$ crystal, the ground state is considered to be a quantum disordered state with a trace of minor spin-glass phase, with magnetic properties being almost identical to those in the $x = 1.5$ crystal. With further hole-doping, dominant magnetic interaction becomes antiferromagnetic [67-69]. Some types of charge order have been reported for $\text{Ca}_{2+x}\text{Y}_{2-x}\text{Cu}_5\text{O}_{10}$ [68,69] and the related system $\text{Ca}_{1-x}\text{CuO}_2$ [70-72]. The possible existence of a spin gap associated with charge order has also been suggested [69].

In the end material $\text{Ca}_2\text{Y}_2\text{Cu}_5\text{O}_{10}$, which contains no holes, the magnetic arrangement in the chain is ferromagnetic. Although quantum fluctuations are considered to be less prominent in a ferromagnetic chain system, the magnetic excitation energy width is known to become broader with increasing Q along the chain as described below. Numerical calculations suggest that magnetic excitations from ferromagnetic chains are strongly affected when a finite antiferromagnetic inter-chain coupling exists or when frustration is introduced between the NN and NNN interactions in the chain [73].

Matsuda *et al.* [74] performed inelastic neutron scattering experiments to study the spin-wave excitations of $\text{Ca}_2\text{Y}_2\text{Cu}_5\text{O}_{10}$ in the AF state. By applying linear spin wave theory on a model Hamiltonian that includes uniaxial anisotropy, magnetic interactions can be determined as shown in Table 1, where the most interesting feature is that the magnetic excitation energy width becomes broader with increasing Q along the chain, although sharp excitations are observed around the zone center and perpendicular to the chain. Broadening of excitation energy width was also reported in a $S=1/2$ 1D Heisenberg ferromagnet $\text{CuCl}_2\cdot\text{DMSO}$ [75], although such broadening is much more pronounced in $\text{Ca}_2\text{Y}_2\text{Cu}_5\text{O}_{10}$. Numerical calculations reveal that the anomalous magnetic excitation spectra in $\text{Ca}_2\text{Y}_2\text{Cu}_5\text{O}_{10}$ are mainly due to antiferromagnetic inter-chain interactions.

Table 1 Magnetic coupling constants in $\text{Ca}_{2+x}\text{Y}_{2-x}\text{Cu}_5\text{O}_{10}$ [76].

x	T (K)	J_{a1} (meV)	J_{ac1} (meV)	D (meV)	J_{ab} (meV)	J_a (meV)	J_b (meV)
0	7	-6.9(1)	1.494(3)	-0.262(3)	0.030(1)	-0.061(6)	0(fixed)
0	20	-6.9(fixed)	1.31(2)	-0.159(2)	0(fixed)	-	0(fixed)
0	25	-6.9(fixed)	1.16(2)	-0.104(2)	0(fixed)	-	0(fixed)
1.5	3	-6.9(fixed)	0.5(fixed)	-0.09(fixed)	0(fixed)	-	0(fixed)
1.67	3	-6.9(fixed)	0(fixed)	0(fixed)	0(fixed)	-	0(fixed)

Neutron scattering experiments were performed on hole-doped $\text{Ca}_{2+x}\text{Y}_{2-x}\text{Cu}_5\text{O}_{10}$ [76]. The systematic study of the hole concentration dependence of the magnetic excitations revealed that magnetic excitations are softened and broadened with increasing temperature or doping holes, irrespective of Q direction, with broadening being larger at higher Q . A characteristic feature is that hole-doping is much more effective to broaden excitations along the chain. As shown in Table 1, although the intra-chain interaction (J_{a1}) does not change so much with increasing temperature or hole-doping, the anisotropic interaction (D) and the inter-chain interaction (J_{ac1}) are reduced. In the spin glass phase ($x = 1.5$) and nearly disordered phase ($x = 1.67$) the magnetic excitations are much broader in energy and Q .

The magnetic properties of $\text{Ca}_{2+x}\text{Y}_{2-x}\text{Cu}_5\text{O}_{10}$ qualitatively resemble those of $(\text{Sr,Ca,La,Y})_{14}\text{Cu}_{24}\text{O}_{41}$. However, from a microscopic standpoint, the sign and absolute value of the intra-chain interaction are different in the two systems (0.20 meV for $\text{Ca}_9\text{La}_5\text{Cu}_{24}\text{O}_{41}$ and -6.9 meV for $\text{Ca}_2\text{Y}_2\text{Cu}_5\text{O}_{10}$), probably due to a slight difference in bond angle and distance between Cu and O [29]. The most characteristic feature is that spin glass behavior is observed in the former system. As the system has no frustrating interactions, yet becomes more one-dimensional with hole-doping, it is difficult to understand how the spin glass phase appears in the absence of frustrating interactions. The spin glass behavior probably appears because finite sized spin clusters, which give rise to cluster spin glass behavior, are formed

due to the rather large intra-chain coupling even with ~30% hole-doping. The neutron scattering study indicates that the magnetic correlation length along the chain is larger than the averaged spin cluster size, which is expected when the holes are randomly distributed. This indicates that there is a possibility of a partial charge ordering, which is consistent with the cluster spin glass model.

3. PHYSICAL PROPERTIES OF TWO-LEG LADDERS IN (Sr, Ca)₁₄Cu₂₄O₄₁ UNDER AMBIENT PRESSURE

This chapter reviews the spin and charge dynamics of two-leg ladders in (Sr, Ca)₁₄Cu₂₄O₄₁. The physical properties of (Sr, Ca)₁₄Cu₂₄O₄₁ dramatically change with chemical substitution at the Sr site [31,34,77]. In spite of a high Cu valence of +2.25, Sr₁₄Cu₂₄O₄₁ shows an insulating behaviour. Metallic behavior is observed by substitution of Ca into Sr_{14-x}Ca_xCu₂₄O₄₁ with $x > 10$. As will be discussed in detail in Sec. 3-2, Ca substitution produces a rearrangement of holes, moving them from the CuO₂ chains into the Cu₂O₃ ladders. As a consequence of interplay between charge and spin degrees of freedom, a variety of ordered states appear, e.g., spin gap state, Néel state, and charge density wave (CDW).

3.1 Spin Gap and AF Ground States in Doped Ladders

La₆Ca₈Cu₂₄O₄₁: ladders without holes : By substituting Sr or Ca with La, the nominal Cu valence can be reduced from +2.25. The magnetic properties of undoped two-leg ladders can be experimentally studied using La₆Ca₈Cu₂₄O₄₁ in which all the Cu atoms are divalent. Neutron scattering [78] and NMR [41] experiments on this compound have confirmed the spin gap ground state. From the T -dependence of ¹⁷O Knight shift, Imai *et al.* [41] estimated the magnitude of the spin gap as $\Delta_{\text{SG}} = 510 \pm 40$ K using

$$\chi(T) \propto \frac{1}{\sqrt{T}} \exp\left(\frac{-\Delta}{k_B T}\right)$$

From the ¹⁷O Knight shift, Imai *et al.* also estimated the exchange coupling constant $J' = 850 \pm 300$ K and $J' / J \sim 0.5$ (J (J') to be the AF exchange coupling constant along the leg (rung)), whereas an inelastic neutron scattering experiment by Matsuda *et al.* [78] reported $J = J' = 110$ meV = 1300 K, and a four-spin exchange interaction $J_{\text{ring}} = 16.5$ meV = 190 K.

Sr₁₄Cu₂₄O₄₁: slightly doped ladders : Several groups have reported results of NMR experiments on Sr₁₄Cu₂₄O₄₁. Tsuji *et al.* [25] estimated the magnitude of a spin gap $\Delta_{\text{SG}} = 470$ K from the nuclear spin-lattice relaxation ratio (T_1) of Cu-NQR, while Magishi *et al.* [27] also measured the ⁶³Cu Knight shift and estimated $\Delta_{\text{SG}} = 550 \pm 30$ K. From NQR results, Takigawa *et al.* [40] estimated $\Delta_{\text{SG}} = 430$ K from the Knight shift and $\Delta_{\text{SG}} = 650$ K from $1/T_1$, respectively (Fig. 3-1). A neutron scattering experiment by Eccleston *et al.* [24] estimated $\Delta_{\text{SG}} = 32.5 \pm 0.1$ meV (~380 K), $J = 130$ meV, and $J' = 72$ meV. Raman scattering experiments have been performed by Sugai *et al.* [79] and Gozar *et al.* [80], with their results indicating agreement and yielding $J = 110 \pm 20$ meV and $J' / J \sim 0.8$.

Distinct from La₆Ca₈Cu₂₄O₄₁, the number of holes residing in the ladders of Sr₁₄Cu₂₄O₄₁ is finite. Takigawa *et al.* [40] found that $1/T_1$ measured by zero-field NQR is dominated by

fluctuations of the electronic field gradient at low temperature, which might be associated with the freezing of the doped holes. Imai *et al.* [41] found that the crossover temperature of the magnetic state from the spin gap regime to the paramagnetic regime occurs at 325 ± 25 K, and suggested that above this temperature the holes frustrate the singlet ground state which eventually transforms the system into a paramagnetic state.

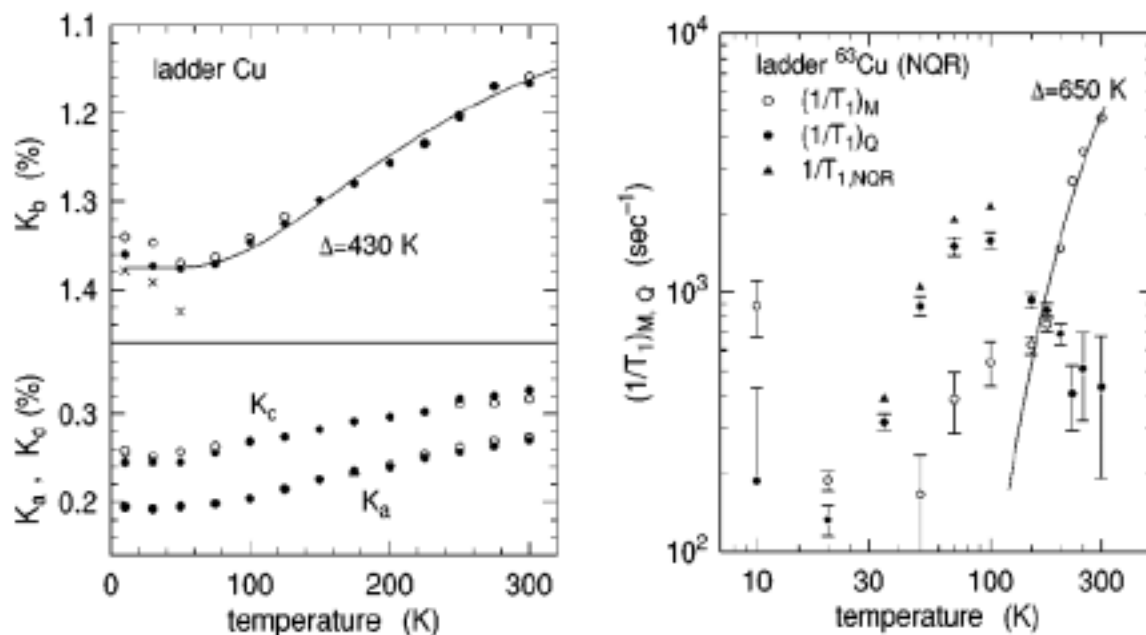


Fig. 3-1 NQR Knight shift and $1/T_1$ for $\text{Sr}_{14-x}\text{A}_x\text{Cu}_{24}\text{O}_{41}$ [40]

$\text{Sr}_{14-x}\text{Ca}_x\text{Cu}_{24}\text{O}_{41}$: *heavily doped ladders*: The magnitude of Δ_{SG} as a function of Ca content x has been measured by NMR and neutron scattering experiments. NMR T_1 -relaxation rate experiments have been carried out by many groups, all of which indicate that Δ_{SG} apparently decreases with increasing x as shown in Fig. 3-2.

On the other hand, a neutron scattering measurement for $x(\text{Ca}) = 11.5$ estimated $\Delta_{\text{SG}} = 32.5 \pm 0.3$ meV (~ 370 K), almost the same magnitude as $x = 0$ [81]. Recently, Fujiyama *et al.* [82] pointed out that the activation energy of $1/T_1$ at the Cu sites is determined by the damping of excitations near $k = (\pi, \pi)$ and may not directly reflect the spin gap.

At a high Ca concentration $x = 11.5$, a long-range magnetic order is observed at low temperatures [83-86], with clear antiferromagnetic transitions having been observed using specific heat measurements (Fig. 3-3). The proposed magnetic structure based on the neutron scattering for a sample with $x = 11.5$ is shown in Fig. 3-4 [87]. The AF ordering temperature increases with increasing Ca content from 2.1 K for $x = 11.5$ to 3.6 K for $x = 13.6$ [85,87]. Remarkably, the singlet ground state and AF ground state coexist in high-Ca substituted samples.

Using a neutron structural analysis and bond valence sum calculation, Isobe *et al.* [88] estimated the hole distribution in the chain and proposed a spin structure which explains observed magnetic Bragg reflections [87].

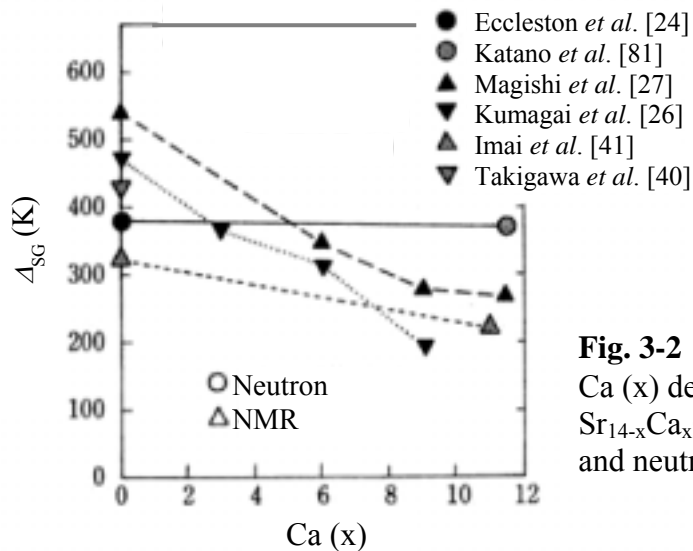


Fig. 3-2
Ca (x) dependence of spin gap Δ_{SG} for $Sr_{14-x}Ca_xCu_{24}O_{41}$ measured by NMR T_1 and neutron scattering.

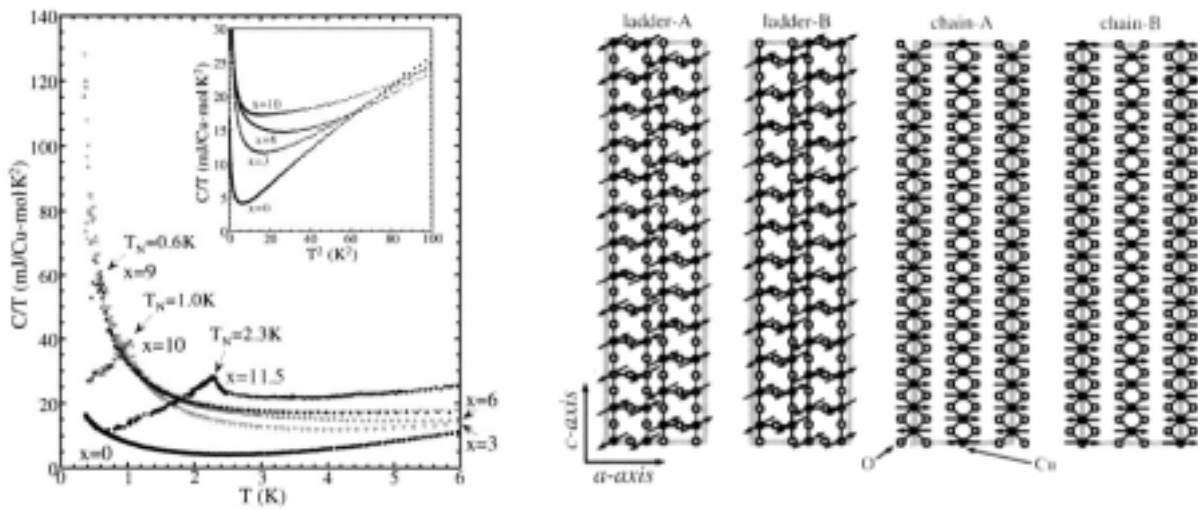


Fig. 3-3
Specific heat data for $Sr_{2.5}Ca_{11.5}Cu_{24}O_{41}$ [87].

Fig. 3-4
The proposed magnetic structure based on the neutron scattering of $Sr_{2.5}Ca_{11.5}Cu_{24}O_{41}$ [87]. Each layer is stacked alternately along b -axis.

3.2 Effect of Ca Substitution

Although Ca^{2+} substitution at the Sr^{2+} site in $(Sr,Ca)_{14}Cu_{24}O_{41}$ does not change the average valence of Cu ions, it dramatically changes the electronic properties. Figure 3-5 shows the resistivity of $(Sr,Ca)_{14}Cu_{24}O_{41}$ single crystals along c - and a -axis.

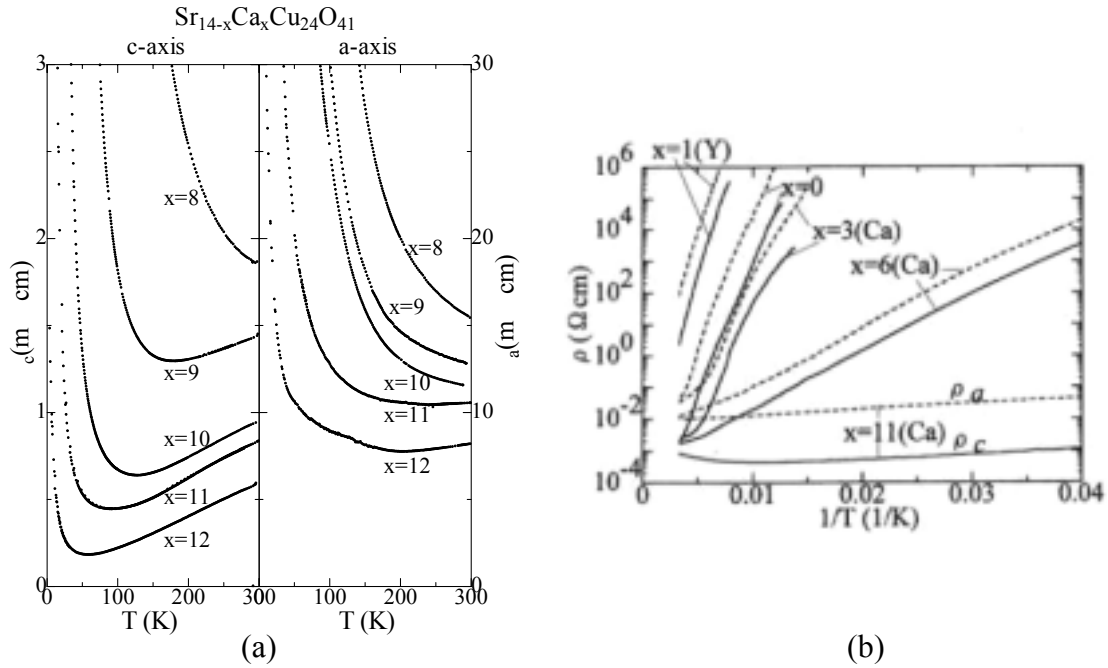


Fig. 3-5 (a) T -dependence of resistivity for $\text{Sr}_{14-x}\text{Ca}_x\text{Cu}_{24}\text{O}_{41}$ along a - and c -directions [89]. (b) The Arrhenius plot of resistivity for $\text{Sr}_{14-x}\text{Ca}_x\text{Cu}_{24}\text{O}_{41}$ and $\text{Sr}_{13}\text{YCu}_{24}\text{O}_{41}$ along a - and c -directions [36].

At $x(\text{Ca}) < 8$, the resistivity shows insulating behavior ($d\rho/dT < 0$) along both directions, whereas at higher $x(\text{Ca}) \sim 9$, resistivity along the c -axis (ρ_c) shows a metallic behavior which is characterized by nearly T -linear dependence above certain T , similar to the in-plane resistivity of high- T_c cuprates at optimal hole doping. Such similar T -dependence and the similar magnitude of resistivity ($\sim 1 \text{ m}\Omega \text{ cm}$) strongly suggest that the conductivity along the c -axis is most likely governed by the 180° Cu-O-Cu networks with strong $\text{Cu}3d\text{-O}2p$ σ bonding, rather than the CuO_2 chains with 90° Cu-O-Cu bonds.

The transition from an insulating to metallic behavior with increasing $x(\text{Ca})$ suggests that Ca substitution results in transferring holes from chains to ladders, with optical conductivity measurements on $(\text{Sr,Ca})_{14}\text{Cu}_{24}\text{O}_{41}$ supporting this picture [49]. Figure 3-6 shows optical conductivity spectra of $(\text{Sr,Ca})_{14}\text{Cu}_{24}\text{O}_{41}$ along the c -axis ($\sigma_c(\omega)$), where the spectrum of the most insulating sample $\text{Sr}_{11}\text{Y}_3\text{Cu}_{24}\text{O}_{41}$ is typical of a charge transfer (CT) insulator, characterized by a peak at 2.0 eV arising from excitation between $\text{Cu}3d$ and $\text{O}2p$ states which is commonly observed in a parent insulators of high- T_c cuprates. Moving to $\text{Sr}_{14}\text{Cu}_{24}\text{O}_{41}$ and further to $(\text{Sr,Ca})_{14}\text{Cu}_{24}\text{O}_{41}$, the conductivity in the low energy region below 1.2 eV increases, while the CT spectral weight decreases, suggesting a spectral weight transfer from a high- to low-energy region similar to that occurring in high- T_c cuprates when a parent insulator is

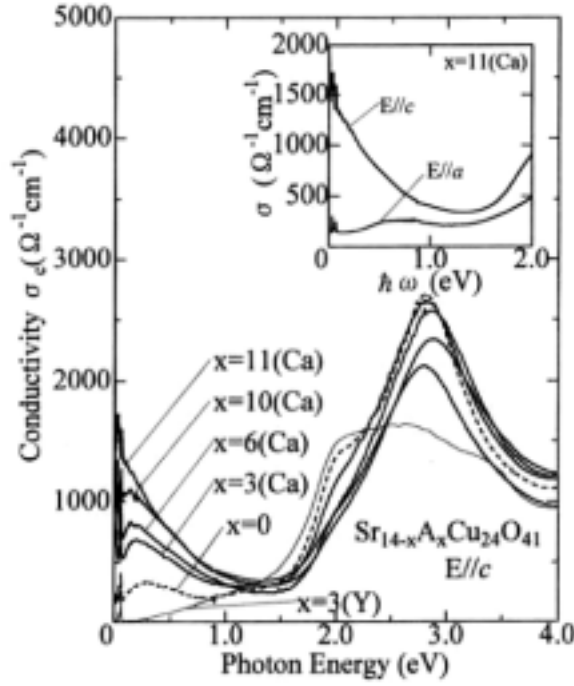


Fig. 3-6 Optical conductivity spectra of $\text{Sr}_{14-x}\text{Ca}_x\text{Cu}_{24}\text{O}_{41}$ along the c -axis ($\sigma_c(\omega)$). The inset shows the anisotropic spectra along a - and c -directions for $x=11$ sample [49].

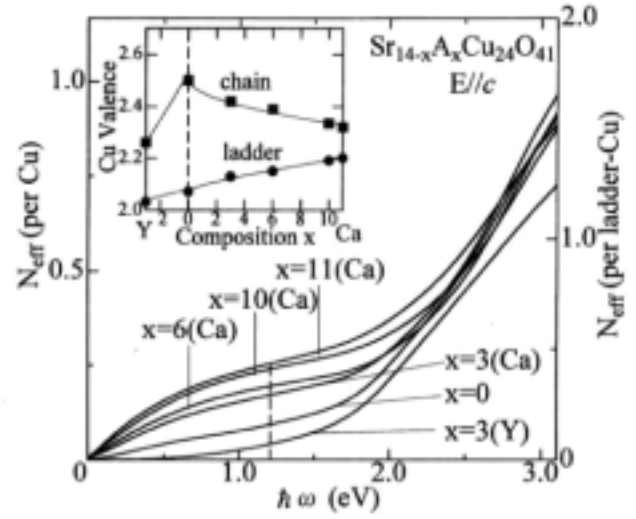


Fig. 3-7 Estimated electron number N_{eff} per Cu (left-hand scale) as a function of energy. N_{eff} per ladder Cu is indicated on the right hand scale. Inset shows the estimated Cu valence of the ladder and the chain [49].

doped with holes. The 3 eV peak does not exist in high- T_c cuprates and decreases with x , which can be attributed to the excitation of doped holes in the CuO_2 chains.

From the optical conductivity spectra, one can estimate the effective electron number participating in the low-energy charge dynamics using

$$N_{eff}(\omega) = \frac{2m_0V}{\pi e^2} \int_0^\omega \sigma_c(\omega') d\omega',$$

where m_0 is the free electron mass, V the volume containing one Cu atom, and $N_{eff}(\omega)$ being proportional to the number of electrons involved in optical excitations up to an energy $\hbar\omega$. The results are shown in Fig. 3-7.

$N_{eff}(\omega)$ takes the same value at 2.5 eV for all $(\text{Sr,Ca})_{14}\text{Cu}_{24}\text{O}_{41}$ samples, indicating that spectral weight transfer takes place in the energy range below 2.5 eV. Assuming that (1) the chain Cu valence is +2.5 for $\text{Sr}_{14}\text{Cu}_{24}\text{O}_{41}$ and (2) the number of holes in Cu_2O_3 ladders is proportional to N_{eff} (1.2 eV), the Cu valence of the ladder and the chain is estimated as shown in the inset of Fig. 3-7. Note that the carrier number of $x = 11$ is as large as 0.2, which corresponds to the hole number of optimally doped high- T_c cuprates.

Takahashi *et al.* [90] performed angle-resolved photoemission spectroscopy experiments on $(\text{Sr,Ca})_{14}\text{Cu}_{24}\text{O}_{41}$ with $x = 0$ and $x = 9$, finding two dispersive features which are attributed to the band dispersion of CuO_2 chains and Cu_2O_3 ladders. Upon Ca substitution, the feature

ascribed to the two-leg ladders approaches the Fermi energy, indicating that the holes are doped into the ladders with Ca substitution.

Using polarization dependent O 1s x-ray absorption spectroscopy on $(\text{Sr,Ca})_{14}\text{Cu}_{24}\text{O}_{41}$, Nücker *et al.* [91] investigated the character of doped holes into the Cu_2O_3 ladders and CuO_2 chains, finding that the holes are doped into O 2p orbitals along the rung upon Ca substitution. They claim that the total hole count in the ladders increases only marginally, being in contrast to results using optical conductivity.

3.3 Anisotropic Charge Dynamics in Metallic Ladders

Figure 3-8 shows the T -dependence of resistivity for $\text{Sr}_3\text{Ca}_{11}\text{Cu}_{24}\text{O}_{41}$ in all three directions, where the inter-ladder resistivity, ρ_a , is 15 to 40 times larger than ρ_c , and the resistivity perpendicular to the ladder plane, ρ_b , is larger than ρ_a by two orders.

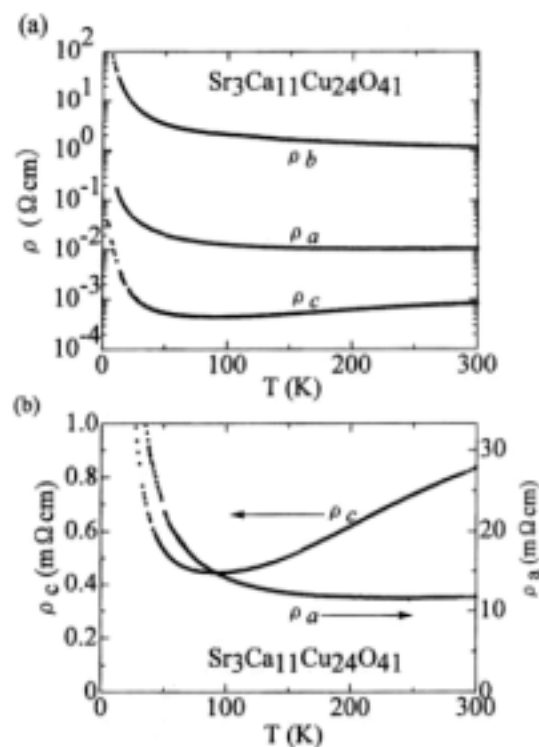


Fig. 3-8
 T -dependence of resistivity for $\text{Sr}_3\text{Ca}_{11}\text{Cu}_{24}\text{O}_{41}$ along all three directions. (a) log-scale. (b) The c - and a -axis resistivity with linear scale [36].

The T -dependence of ρ_a (and also ρ_b) is anomalous in that ρ_a is insulating ($d\rho_a/dT < 0$) in the temperature range where ρ_c shows metallic behavior ($d\rho_c/dT > 0$). Such contrasting T -dependence between intra- and inter-ladder conduction is analogous to that observed between in-plane (ρ_a) and out-of-plane (ρ_c) resistivity in underdoped high- T_c cuprates.

The anisotropic charge dynamics has been further investigated by optical measurements. Figure 3-9 shows optical conductivity along the a -axis ($\sigma_a(\omega)$) for $x = 8$ and $x = 11$ at various temperatures, where for both x values the low-energy spectral weight is transferred to high energies when the sample is cooled down. This behavior is similar to the “pseudogap” observed in interplane optical conductivity ($\sigma_c(\omega)$) of high- T_c cuprates such as YBCO and LSCO in the under doped region [92]. Obviously then, the insulating resistivity along the a -

axis originates from the suppression of low-energy conductivity due to opening the pseudogap in $\sigma_a(\omega)$.

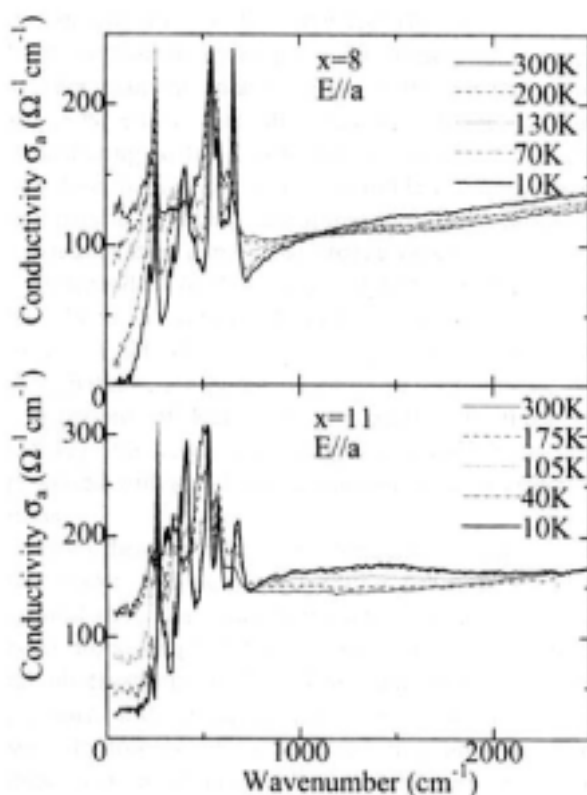


Fig.3-9 a -axis optical conductivity for $\text{Sr}_{14-x}\text{Ca}_x\text{Cu}_{24}\text{O}_{41}$ ($x = 8$ and 11) [93].

The energy scale of the pseudogap is $\sim 1100 \text{ cm}^{-1}$ (140 meV) for $x = 8$ and $\sim 600 \text{ cm}^{-1}$ (74 meV) for $x = 11$. The magnitude of the pseudogap is comparable with that in high- T_c materials, e.g., 600 cm^{-1} for $\text{YBa}_2\text{Cu}_3\text{O}_{6.70}$, presumably reflecting the same microscopic origin [92]. NMR experiment shows that the temperature below which a spin gap opens in doped ladders ($x = 11.5$) coincides with the temperature where ρ_a starts to show negative T -dependence, indicating that the spin gap has a close connection with the optical pseudogap [27].

Figure 3-10 shows that in contrast to the pseudogap in $\sigma_a(\omega)$, the c -axis optical conductivity $\sigma_c(\omega)$ is characterized by a low energy peak which rapidly grows with decreasing T , where the peak in $\sigma_c(\omega)$ is located at $\sim 100 \text{ cm}^{-1}$ for $x = 8$, and $\sim 50 \text{ cm}^{-1}$ for $x = 11$. The peak is distinct from a Drude peak of free carriers since it is located at finite energies and develops when ρ_c shows insulating behavior.

The observed peak in $\sigma_c(\omega)$ can be interpreted to be a signature of a collective mode of a pinned charge-density wave (CDW). First of all, peak width in $\sigma_c(\omega)$ is quite narrow, suggestive of a well-defined collective mode, and secondly the T -dependence of the peak intensity follows a BCS gap equation which is an expected formula for CDW systems. In this framework the pseudogap in $\sigma_a(\omega)$ signals a formation of hole pairs that would be confined

within a ladder and unable to hop between ladders. The T -dependence of $\sigma_c(\omega)$ and $\sigma_a(\omega)$ indicate that the holes are progressively paired with decreasing T and the pairs readily form a short-range charge order which is locally pinned by impurities and/or lattice imperfections.

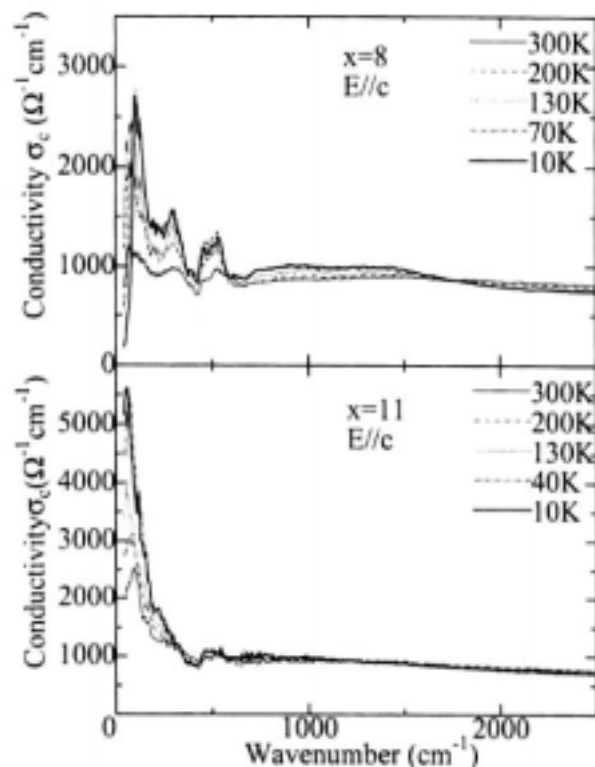


Fig.3-10 c -axis optical conductivity for $\text{Sr}_{14-x}\text{Ca}_x\text{Cu}_{24}\text{O}_{41}$ ($x = 8$ and 11) [93]

For $x = 8$, the collective mode is strongly pinned at finite energy $\sim 100 \text{ cm}^{-1}$ and does not contribute to the DC conductivity, resulting in an insulating behavior. For $x = 11$, CDW may be de-pinned by thermal fluctuations and therefore contribute to metallic conduction along the c -axis. On the other hand, across the ladders, a hole pair must be dissociated into two single holes by thermal excitation across the gap, thus resulting in an insulating a -axis transport.

Independent of the above studies, there has been systematic optical studies by Ruzicka *et al.* [94] on $\text{Sr}_{14-x}\text{Ca}_x\text{Cu}_{24}\text{O}_{41}$ ($x=0, 5$ and 12). Although some quantitative differences exist, conclusions are consistent with each other.

3.4 Charge Order in $\text{Sr}_{14}\text{Cu}_{24}\text{O}_{41}$

The charge dynamics of $\text{Sr}_{14}\text{Cu}_{24}\text{O}_{41}$ (and small Ca substituted samples) is quite different from its higher- x counterpart. As shown in Fig. 3-5, the resistivity of $\text{Sr}_{14}\text{Cu}_{24}\text{O}_{41}$ indicates an insulating behavior both along the c - and a -axis. Kitano *et al.* [95] found a dramatic increase of microwave conductivity below 170 K. Detailed study of the frequency dependence of the conductivity revealed the existence of a sharp resonance-like peak around 55 GHz (~ 0.2

meV). Since the peak frequency is much smaller than the thermal energy per carrier, this peak is attributed as a resonance mode of some collective charge excitation, similar to the pinned phase mode of charge- and spin- density wave (C/SDW) systems [96]. Similar nonlinear conduction was also observed by Gorshunov *et al.* [97,98], while subsequent Raman scattering and AC conductivity measurements by Blumberg *et al.* [99] have strengthened this picture. It should be noted that C/SDW correlation in $\text{Sr}_{14}\text{Cu}_{24}\text{O}_{41}$ persists up to 630 K, indicating that charge-spin correlations do not arise from phonons as in usual C/SDW systems, but rather from interactions stronger in energy such as in AF exchange or Coulomb interaction. Optical conductivity measurements on $\text{Sr}_{14}\text{Cu}_{24}\text{O}_{41}$ revealed that the transfer of spectral weight is extended to a high energy up to the CT gap, which suggests that C/SDW in $\text{Sr}_{14}\text{Cu}_{24}\text{O}_{41}$ involves a very large energy scale comparable to Coulomb energy.

Hess *et al.* [100] and Kudo *et al.* [101] showed that thermal conductivity ($\kappa(T)$) is useful to investigate interactions between the magnetic excitations and charge dynamics of doped holes, finding that the T -dependence of the magnon mean free path, l_{mag} in ladders correlates with the mobility of holes. In particular, they found a drastic enhancement of l_{mag} associated with the charge order in ladders.

4. PHYSICAL PROPERTIES OF TWO-LEG LADDERS IN $(\text{Sr, Ca})_{14}\text{Cu}_{24}\text{O}_{41}$ UNDER HIGH PRESSURE

4.1 The Discovery of Pressure-Induced Superconductivity in Two-Leg Ladder Compound $\text{Sr}_{0.4}\text{Ca}_{13.6}\text{Cu}_{24}\text{O}_{41.84}$

Superconductivity in ladder material was first discovered by Uehara *et al.* [11] in two-leg ladder compound $\text{Sr}_{0.4}\text{Ca}_{13.6}\text{Cu}_{24}\text{O}_{41.84}$. They found that the solubility limit of Ca ions, or the hole-doping limit into Cu_2O_3 ladders, can be extended up to $x=13.6$ by synthesizing samples under high- O_2 pressure. The recipe for synthesizing polycrystal samples adopted by Uehara *et al.* follows.

A sample with nominal composition $\text{Sr}_{0.4}\text{Ca}_{13.6}\text{Cu}_{24}\text{O}_{41}$ was synthesized from SrCO_3 , CaCO_3 , and CuO powders with purities higher than 99.9%. The powder mixture was calcined at 1000 °C for 50 h under flowing O_2 using four intermediate grindings. The resultant powders were then formed into pellets and sintered using a HIP furnace at 1200 °C for 8 h under 20% O_2 + 80% Ar at a total pressure of 2000 atm. Oxygen content was determined by the inert gas fusion-infrared absorption method.

Figure 4-1 shows the x-ray powder diffraction pattern of $\text{Sr}_{0.4}\text{Ca}_{13.6}\text{Cu}_{24}\text{O}_{41.8}$, where all peaks are indexed indicating the sample is single phase. At ambient pressure the lattice parameters a , b , and c are 11.14, 12.44, and 27.02 Å, respectively. Because the 1D-chain and ladder are linked incommensurately, the c -axis length could only be calculated using $(0\ 0\ 7n)$ ($n = \text{integer}$) reflections which indicate the c -axis length of the ladder.

Figure 4-2 shows the T -dependent electrical resistivity of a polycrystal sample under a pressure (P) of 0, 1.5, 2, and 3 GPa, where the magnitude of electrical resistivity at room temperature decreases monotonically with increasing pressure. The electrical resistivity at 0 and 1.5 GPa is almost flat above 200 K and shows a broad maximum at ~110 K. A similar broad peak has also been observed in the nearly metallic ladder compound

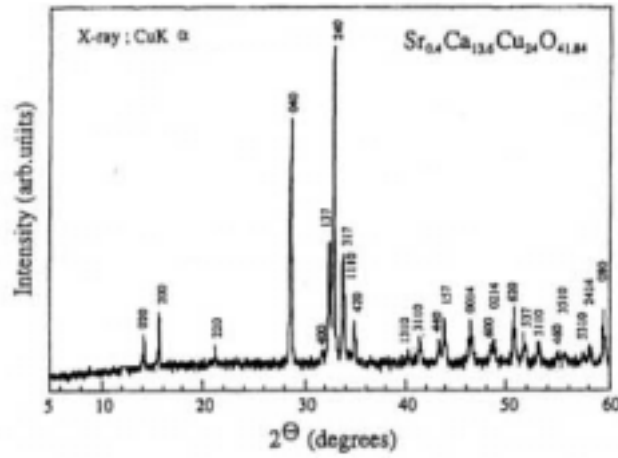


Fig. 4-1 x-ray powder diffraction pattern of $\text{Sr}_{0.4}\text{Ca}_{13.6}\text{Cu}_{24}\text{O}_{41.84}$

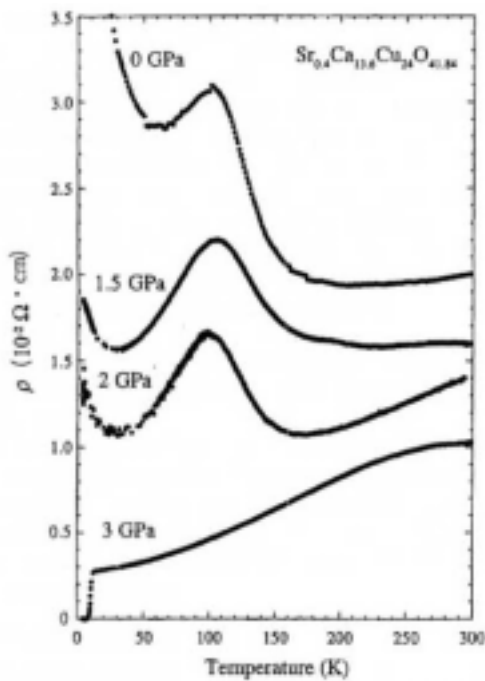


Fig. 4-2 T -dependence of the electrical resistivity of $\text{Sr}_{0.4}\text{Ca}_{13.6}\text{Cu}_{24}\text{O}_{41.84}$ under pressure of 0, 1.5, 2 and 3 GPa [11].

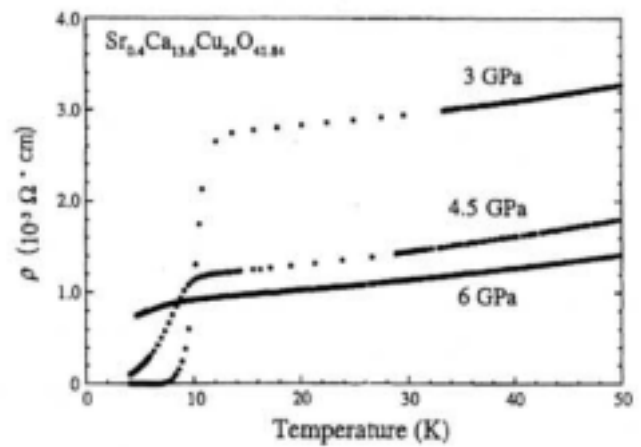


Fig. 4-3 T -dependence of the electrical resistivity of $\text{Sr}_{0.4}\text{Ca}_{13.6}\text{Cu}_{24}\text{O}_{41.84}$ under pressure of 3, 4.5 and 6 GPa below 50 K [11].

($\text{Sr}_{0.4}\text{Ca}_{0.6}$) $_{14}\text{Cu}_{19.2}\text{Co}_{4.8}\text{O}_{41}$ [102] and was thought to be a characteristic feature of this system when it is close to the metallic state. Such behavior is now considered to be extrinsic, possibly arising from the “parallel circuit” effect of polycrystal samples. As discussed in Chap. 3, in high-Ca samples the resistivity is anisotropic, being metallic along the c -axis and insulating along the a - and b - axis. In polycrystal samples the resistance of the sample is the combined parallel circuit resistance of ρ_a and ρ_c , such that a broad peak appears at the temperature where the difference between ρ_a and ρ_c becomes very large. The electrical resistivity increases again below ~ 60 and ~ 30 K at 0 and 1.5 GPa, respectively. The T -dependence of the electrical resistivity at 2 GPa is metallic above 150 K and shows similar behavior to that at 1.5 GPa below 150 K. The superconducting transition occurs at 12.5 K at 3 GPa with metallic behavior above T_c , and the zero resistivity temperature is 8 K. Figure 4-3 shows the T -dependence of the electrical resistivity at 3, 4, and 6 GPa below 50 K. It is clear that the value of T_c (onset) decreases from 12.5 to 9 K with increasing P from 3 to 4.5 GPa. Finally, the superconducting transition disappears under an applied pressure of 6 GPa. Note that the effect of pressure observed in this compound is much larger than in any other high- T_c cuprates in which application of pressure by itself does not cause insulator-superconductor-metal transition without changing the doping concentration.

As discussed in Chap. 3, Ca substitution leads to redistribution of hole carriers from the 1D chain to ladder plane [49]. As the Ca^{2+} ion is smaller than that of Sr^{2+} , the substitution of a Ca ion results in (chemical) pressure applied to the system. It is therefore reasonable that the role of pressure is essentially the same as Ca substitution and causes further hole-doping into the ladder plane. Under this hypothesis, the critical hole concentration for superconductivity is achieved only when physical and chemical pressures are applied. However, this postulation may turn out to be insufficient for understanding the role of pressure in the emergence of superconductivity, as will be discussed in Sec. 4.4 based on experimental results using a single crystal.

4.2 Crystal Structure under High Pressure

In order to confirm bulk superconductivity in $\text{Sr}_{0.4}\text{Ca}_{13.6}\text{Cu}_{24}\text{O}_y$, Isobe *et al.* [103] examined the crystal structure of $\text{Sr}_{0.4}\text{Ca}_{13.6}\text{Cu}_{24}\text{O}_{41.84}$ at high P and low T . They concluded using x-ray diffraction results that the $\text{Sr}_{0.4}\text{Ca}_{13.6}\text{Cu}_{24}\text{O}_y$ phase persists at least up to 9 GPa and down to 7 K without serious decomposition or phase transition.

Figure 4-4 shows x-ray diffraction patterns at various P and T , where a comparison of the diffraction pattern at ambient pressure and room temperature indicates there is no significant difference in the x-ray pattern at $P = 5$ GPa and $T = 7$ K when the sample is in the superconducting state. In addition to primary reflections, an extra peak, which increases its intensity at high P is observed as indicated by arrows. Isobe *et al.* considered the extra peak to be a higher-order satellite caused by a slight structural modulation. It has therefore been concluded that superconductivity actually comes from $\text{Sr}_{0.4}\text{Ca}_{13.6}\text{Cu}_{24}\text{O}_{41.84}$ and not from any impurity phase stabilized under high pressure.

Figure 4-5 shows P -dependent lattice constants measured at room temperature, where lattice constants smoothly decrease with increasing P . Of particular interest, it is clear that the compression rate of the b -axis is the largest among three axes (0.73%/GPa). This trend is similar to Ca-substitution dependence of lattice parameters; a similarity that suggests external pressure plays the same role as Ca substitution, i.e., transferring hole carriers from the CuO_2

chains to the Cu_2O_3 ladders through the hybrid orbitals of $\text{Cu}_{1\text{Dchain}}\text{-O}_{1\text{Dchain}}\text{-Cu}_{\text{ladder}}$. Precise crystal structure analysis using a super-symmetric group has indeed shown that the oxygen atoms of 1D chains displace towards the ladder and act as apical oxygen in $\text{Cu}_{\text{ladder}}$ [45,104]. Such an apical oxygen probably works as the pathway for hole-redistribution from the 1D chain to the ladder.

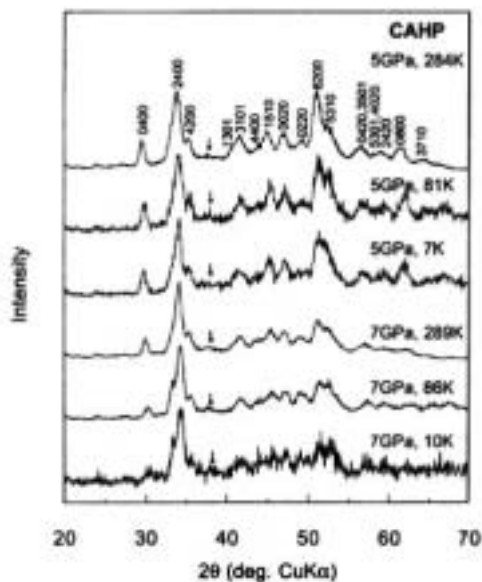


Fig. 4-4 The x-ray diffraction patterns of $\text{Sr}_{0.4}\text{Ca}_{13.6}\text{Cu}_{24}\text{O}_y$ at various pressure and temperature. The weak extra peak is shown by arrows [103].

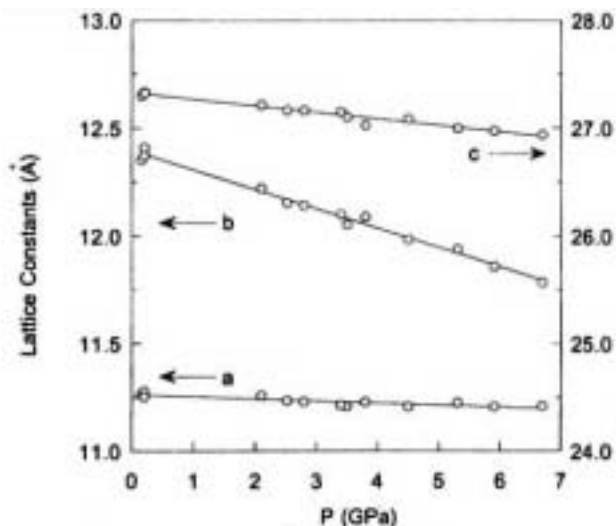


Fig. 4-5 The pressure dependence of lattice constants of $\text{Sr}_{0.4}\text{Ca}_{13.6}\text{Cu}_{24}\text{O}_y$ at room T [103].

The above discussion based on high- P x-ray studies is summarized as follows: (1) there is no significant P -induced structural change and/or phase decomposition which confirms bulk superconductivity in $\text{Sr}_{0.4}\text{Ca}_{13.6}\text{Cu}_{24}\text{O}_y$, and (2) external pressure results in shrinking the lattice parameters especially along the b -axis. Accordingly, the effect of Ca substitution and external pressure are quite similar to each other.

4.3 Evolution of Spin Gap of $(\text{Sr,Ca})_{14}\text{Cu}_{24}\text{O}_{41}$ with Pressure

As described in the Chap. 3, the magnitude of the spin gap, Δ_{SG} , decreases with Ca substitution, i.e., hole-doping into the ladder. According to Magishi *et al.*'s [27] data of a ^{63}Cu Knight shift, for example, the spin gap decreases with Ca-doping from $\Delta_{\text{SG}} = 550 \pm 30$ K for $\text{Sr}_{14}\text{Cu}_{24}\text{O}_{41}$ to 350 ± 30 K, 280 ± 30 K, and 270 ± 30 K for $x = 6, 9$ and 11.5 , respectively. A more interesting issue is how the spin gap evolves under pressure at which the sample is in a superconducting state.

High- P NMR measurements were first performed by Mayaffre *et al.* [105] on $\text{Sr}_2\text{Ca}_{12}\text{Cu}_{24}\text{O}_{41}$, showing a superconducting transition at 5 K and 3 GPa. Based on experimental data, they concluded that the spin gap collapses at $P > 3$ GPa and a superconducting phase sets in. Results, however, were based on extracted data in the normal

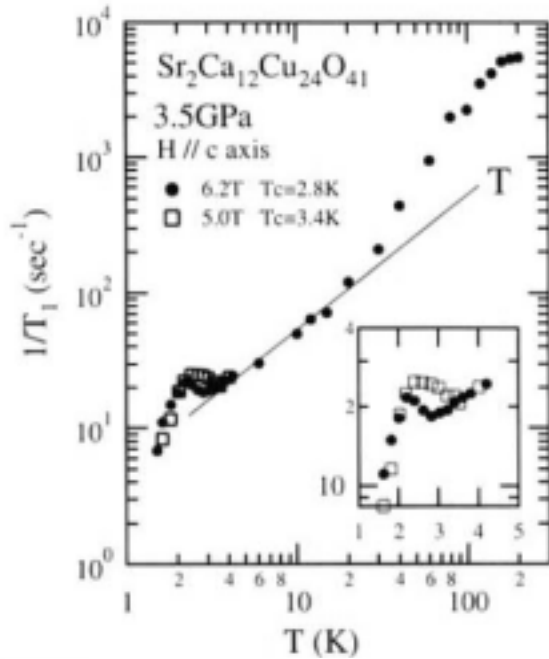


Fig. 4-6 Nuclear magnetic relaxation rate $1/T_1$ for ^{63}Cu nuclei. The solid line shows Korringa relation. $1/T_1$ at low temperature around T_c is expanding as indicated in the inset [108].

[109]; a behavior that occurs due to hole doping and whose pairing likely causes superconductivity. If true, the spin-gap formation observed from T_1^{-1} at high temperature would not contribute to the pairing formation of superconductivity. It is also pointed out that (i) the spin fluctuation of a $\text{Sr}_{14-x}\text{Ca}_x\text{Cu}_{24}\text{O}_{41}$ system measured by NMR is much smaller than that in 2D high- T_c cuprates [108], and (ii) the T_c of these materials might be scaled by the magnitude of the spin fluctuation, rather than by the energy scale of the spin gap.

High- P inelastic neutron scattering experiments for $\text{Sr}_{2.5}\text{Ca}_{11.5}\text{Cu}_{24}\text{O}_{41}$ were performed by Katano *et al.* [81], where in contrast to NMR results, they found Δ_{SG} does not change with Ca substitution. Moreover, even under pressure, Δ_{SG} remains unchanged and takes the same value of ~ 33 meV similar to undoped material $\text{Sr}_{14}\text{Cu}_{24}\text{O}_{41}$.

4.4 Evolution of Electrical Properties of $\text{Sr}_{2.5}\text{Ca}_{11.5}\text{Cu}_{24}\text{O}_{41}$ Single Crystal with Pressure

As described in Chap. 3, the charge dynamics of $\text{Sr}_{14-x}\text{Ca}_x\text{Cu}_{24}\text{O}_{41}$ is quite anisotropic under ambient pressure. To understand the charge dynamics in the superconducting phase, it is helpful to evaluate how inter-ladder coupling evolves with P . Anisotropic electrical resistivity measurements under high P were carried out by Nagata *et al.* [110] using a single crystal of $\text{Sr}_{2.5}\text{Ca}_{11.5}\text{Cu}_{24}\text{O}_{41}$. Figure 4-7 shows T -dependence of resistivity, ρ_c and ρ_a , of $\text{Sr}_{2.5}\text{Ca}_{11.5}\text{Cu}_{24}\text{O}_{41}$ at various P up to 4.5 GPa. At ambient pressure, ρ_c shows metallic T -dependence above ~ 100 K, and applying P causes both ρ_c and ρ_a to decrease. The insulating behavior observed at low T is weakened with increasing P , nearly vanishing at 4.5 GPa, while simultaneously a superconducting transition sets in at 9 K. Note that the superconducting

state above T_c . Piskunov *et al.* [106,107] performed similar experiments and obtained similar results. Recently, Fujiwara *et al.* [108] performed precise NMR measurement with an improved high- P technique using a large, high-quality crystal of $\text{Sr}_2\text{Ca}_{12}\text{Cu}_{24}\text{O}_{41}$. Figure 4-6 shows the T -dependence of T_1^{-1} , where the spin gap appears even under high P as an activated T -dependence of T_1^{-1} at $T > 30$ K. Δ_{SG} is estimated to be 173 K. Near T_c (2.8 K under 6.2 T and 3.4 K under 5.0 T), a peak occurs which the authors interpret to be a superconducting coherence peak, i.e., there is a finite gap in the quasiparticle excitation indicating that the superconductivity possesses an s -wave-like character. At a pressure of 3.5

GPa and below 30 K, a T -linear component in T_1^{-1} was observed versus an activation-type one. The authors attributed this gapless mode to the free motion of holon-spinon bound states

ground state emerges from the insulating ground state without going through the non-superconducting metallic region; a behavior that is quite similar to that of high- T_c superconductors in which superconductor- to insulator (SI) transition takes place when some impurities such as Zn ions are doped in the CuO_2 planes [111]. At P higher than 5 GPa [inset of Fig.4-7(a)], T_c starts to decrease, being qualitatively consistent with previous results using polycrystal samples.

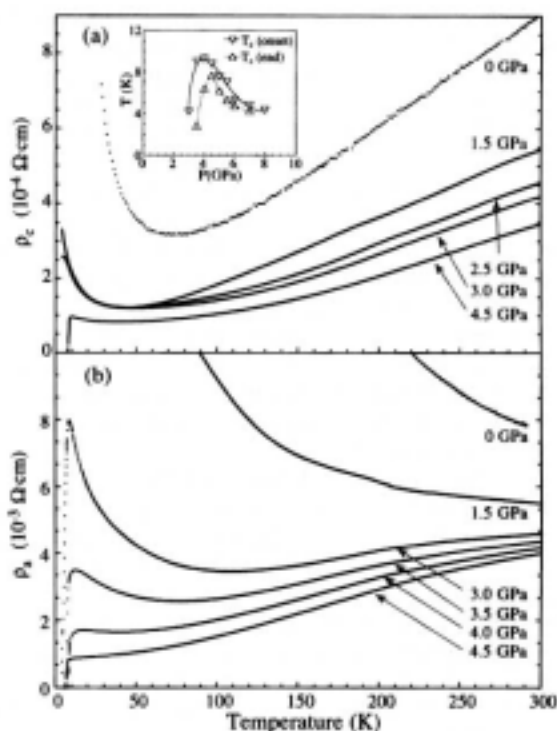


Fig. 4-7 Effect of pressure on temperature dependence of the resistivity (a) along the ladder direction (ρ_c) and (b) across (perpendicular to) the ladder in the ladder plane (ρ_a) of single crystal $\text{Sr}_{2.5}\text{Ca}_{11.5}\text{Cu}_{24}\text{O}_{41}$ at indicated pressure. Inset shows the pressure dependence of T_c [110].

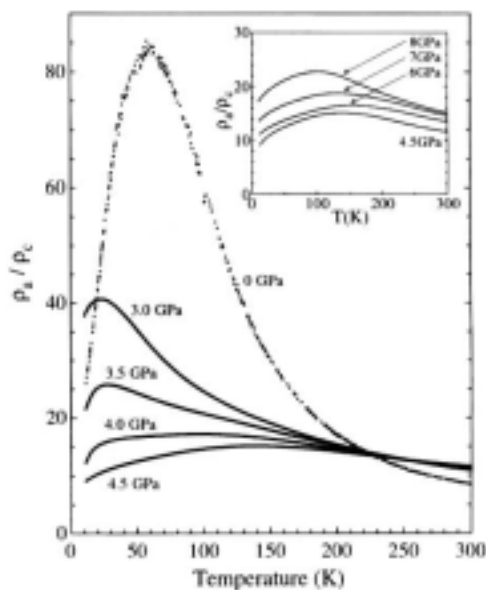


Fig. 4-8 Effect of pressure on temperature dependence of the anisotropic ratio ρ_a/ρ_c of single crystal $\text{Sr}_{2.5}\text{Ca}_{11.5}\text{Cu}_{24}\text{O}_{41}$ at indicated pressure. Inset shows the anisotropic ratio ρ_a/ρ_c above 4.5 GPa [110].

At ambient P , ρ_a shows an insulating behavior with negative T coefficient, indicating incoherent charge dynamics across the ladders. By applying pressure, the T coefficient crosses over from negative to positive such that the temperature region of the positive T coefficient widens. At $P > 4.5$ GPa, ρ_a shows metallic behavior all the way down to T_c , which indicates that high P induces concomitant occurrence of superconductivity and coherent charge dynamics perpendicular to the ladders. One may consider that the decrease in ρ_a and ρ_c results from hole-doping into the ladders, i.e., by transfer from the 1D chain to ladder plane, similar to Ca substitution. However, a clear difference exists between the application of external pressure and Ca substitution in that with Ca substitution the anisotropy ρ_a/ρ_c is

enhanced (see Fig. 3-5(a)), whereas external pressure *reduces* the anisotropy so as to realize 2D metallic charge transport under high P .

Figure 4-8 shows the temperature dependence of anisotropy ratio ρ_a/ρ_c at various pressures, where the ρ_a/ρ_c at room temperature is about 10 and almost independent of P . With decreasing T at ambient pressure, ρ_a/ρ_c increases, reaching a maximum value of 85 at 50 K due to metallic ρ_c and insulating ρ_a . Application of external pressure suppresses the enhancement of ρ_a/ρ_c at low T . Finally, ρ_a/ρ_c becomes nearly T independent above ~ 4.0 GPa where superconductivity sets in.

To summarize the single crystal transport experiment by Nagata *et al.* [110], the application of pressure causes not only effective carrier doping into the ladder but also dimensional crossover in the charge dynamics from one to two, and superconductivity of the ladder appears on the 2D electrical background rather than 1D.

4.5 Pressure Effect in the Low Ca Region

Systematic high- P resistivity measurements at various x have been carried out by Motoyama *et al.* [112]. Even under high P , compounds with $x < 8$ continue to be insulating except for $x=0$ which undergoes an insulator-to-metal transition, presumably due to the distraction of the charge-ordered state. On the other hand, for $x > 10$, a superconducting transition occurs at $P \sim 3\text{--}5$ GPa. Based on these experimental results and extrapolated behavior to $T = 0$ K, the x - P phase diagram of $\text{Sr}_{14-x}\text{Ca}_x\text{Cu}_{24}\text{O}_{41}$ can be drawn as shown in Fig. 4-9.

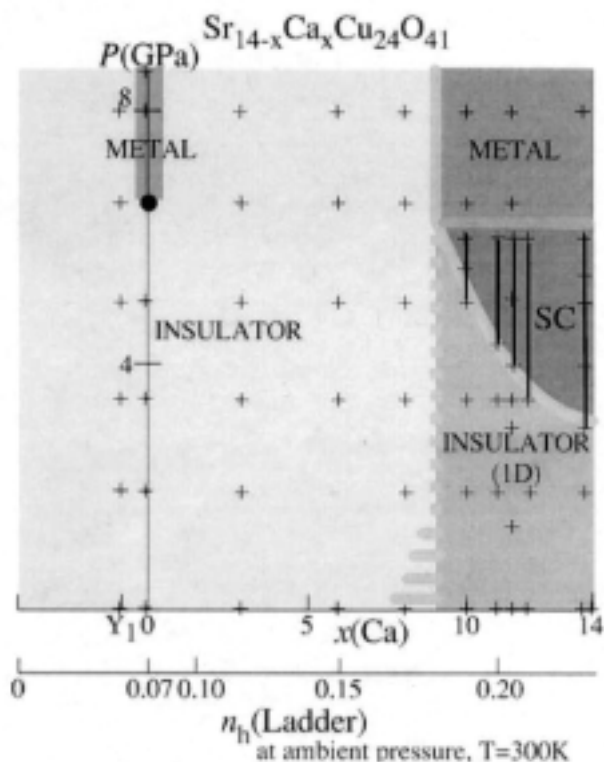


Fig. 4-9

The x - P phase diagram of $\text{Sr}_{14-x}\text{Ca}_x\text{Cu}_{24}\text{O}_{41}$. Crosses represent points where measurements have been carried out.

The crossover in the nature of the insulating state is indicated by a thick-dashed vertical line. The superconducting phase is restricted at high P and for $x > 10$ [89].

For $x = 10$, there is a temperature region where $d\rho_c/dT > 0$ and $d\rho_a/dT < 0$, whereas for $0 < x < 8$, both ρ_c and ρ_a always show a negative T coefficient at any P below 300 K. These results suggest the existence of two distinct insulating phases in $\text{Sr}_{14-x}\text{Ca}_x\text{Cu}_{24}\text{O}_{41}$ with a boundary at $x \sim 8$. Apparently, the different nature of the two insulating phases might be related to the occurrence and non-occurrence of superconductivity at high P .

4.6 Upper Critical Field under Pressure

Nakanishi *et al.* described the superconducting upper critical magnetic field, $H_{c2}(T)$, in a $\text{Sr}_{14-x}\text{Ca}_x\text{Cu}_{24}\text{O}_{41}$ ($x = 12$) single crystal with $T_c \sim 5$ K at $P = 3.0$ GPa [113]. They measured the T -dependence of AC susceptibility at 4.0 GPa in magnetic fields applied along the a -, b -, and c -axis, determining $H_{c2}(T)$ for these three directions down to about 1.6 K.

Figure 4-10 shows the T -dependence of $H_{c2}(T)$ for directions $H_{a_{c2}}$ (H parallel to a), $H_{b_{c2}}$ (H parallel to b), and $H_{c_{c2}}$ (H parallel to c), where T -dependence of H_{c2} is different in that $H_{a_{c2}} > H_{c_{c2}} > H_{b_{c2}}$ within the measured temperature range. This result indicates that the superconducting state is anisotropic and that the coherence length, ξ , has the following relation, $\xi_a > \xi_c > \xi_b$, i.e., the shortest coherence length among three directions is the b -axis, which is consistent with that expected from a layered crystal structure.

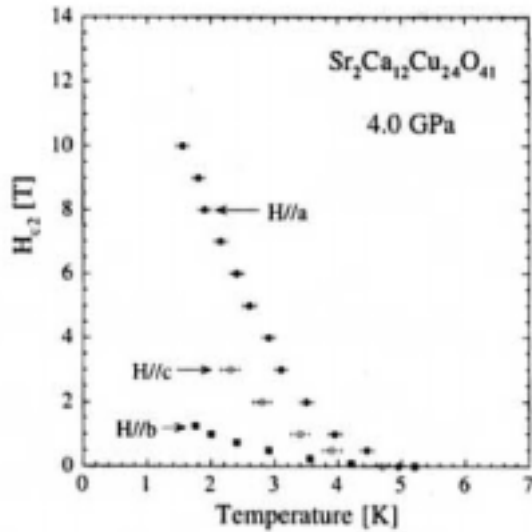


Fig. 4-10
 T -dependence of the upper critical field, $H_{c2}(T)$ of $\text{Sr}_2\text{Ca}_{12}\text{Cu}_{24}\text{O}_{41}$ at 4.0 GPa for H parallel a - (closed circles), b - (closed squares) and H parallel c -axis (open circles) [113].

However, the relation $\xi_a > \xi_c$ is not considered appropriate in that superconducting coherence along the a -axis is stronger than that along the c -axis, or that the electronic bandwidth in the normal state is larger along the a - than c -axis. This conflicts with conductivity measurements showing ρ_a/ρ_c is about 15 from 300 ~ 4.2 K at 4 GPa, i.e., conductivity along the c -axis is clearly higher than the a -axis [110]. Further experimental and theoretical efforts are need to clarify the point.

5. SUMMARY ON SPIN GAP AND SUPERCONDUCTIVITY OF TWO-LEG LADDER

In the spin ladder compound $\text{Sr}_{14-x}\text{Ca}_x\text{Cu}_{24}\text{O}_{41}$, experiments indicate that (1) Ca substitution corresponds to hole carrier doping into the two-leg ladder through hole-charge redistribution from the CuO_2 chain to the ladder, (2) spin gap as predicted by theory exists, and (3) superconducting transition occurs with $x = 11.5$ and at applied pressure higher than ~ 3 GPa. Accordingly, the basic phase diagram of $\text{Sr}_{14-x}\text{Ca}_x\text{Cu}_{24}\text{O}_{41}$ can be described as shown in Fig. 5-1 (Magishi *et al* [27], see Fig. 4-9 also).

In addition to the basic properties of $\text{Sr}_{14-x}\text{Ca}_x\text{Cu}_{24}\text{O}_{41}$ represented in Fig. 5-1, novel single crystal transport and NMR measurements under high- P have newly revealed relevant information such that it is now possible to expand discussions on the physics of $\text{Sr}_{14-x}\text{Ca}_x\text{Cu}_{24}\text{O}_{41}$. These recent experimental results allow us further discussions on the origin of superconductivity in the ladder compounds.

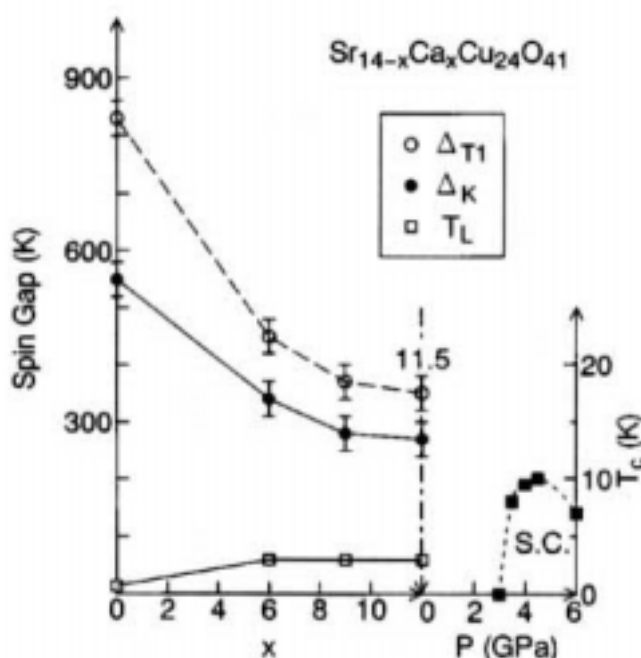


Fig. 5-1

Phase diagram of $\text{Sr}_{14-x}\text{Ca}_x\text{Cu}_{24}\text{O}_{41}$ as functions of x and pressure. The spin gaps Δ_K () and Δ_{T1} () are obtained from the Knight shift and the T_1 measurements, respectively. T_c of $x=11.5$ sample is also plotted by solid squares (scale on right axis). See ref. [27] for more detail.

(1) spin gap

It has been theoretically predicted that spin gap remains finite against carrier doping and that superconductivity appears by taking advantage of spin gap. The magnitude of the spin gap has been predicted to decrease by carrier doping [1], while NMR experiments provide

evidence that Δ_{SG} decreases by carrier doping at ambient pressure, being consistent with theoretical predictions. Neutron experiments, however, reveal that Δ_{SG} is almost unchanged. The reason for the discrepancy between NMR and neutron experiments remains unclear. It should be noted that these two methods observe spin excitations with different wave vector k , which could be one explanation for such differences.

High- P NMR measurements demonstrate that spin gap behavior crosses over to a gap-less Korringa-like behavior above T_c (3–30 K). Such results can be interpreted to indicate that the free motion of holon-spinon bound states could be the origin of gap-less state, i.e., the spin gap survives in the superconducting state although it does not provide the crucial contribution to superconductivity [108]. Inelastic neutron scattering experiments at $P = 2.1$ GPa for $x = 11.5$ sample confirmed the existence of spin gap [81], where this pressure is close to the critical pressure for the emergence of superconductivity, suggesting that the spin gap might survive even under high P where the superconducting ground state exists at low T .

(2) Superconductivity

It has been theoretically predicted that superconductivity in ladder systems emerges due to the formation of electron (hole) pairs created by minimizing the energy-loss from breaking spin singlet pairs. The magnitude of the spin gap is on the order of hundreds of degrees Kelvin. Such a high energy scale leads us to expect high- T_c superconductivity in the ladder materials which has indeed triggered extensive experimental material research. However, the highest T_c of the existing ladder material is thus far limited to 12.5 K, being an order of magnitude smaller than 2D high- T_c cuprates, which suggests that the origin of superconductivity in real materials is not exactly the same as that expected from the simple spin gap-mediated superconductivity mechanism.

From single crystal resistivity experiments we know that external pressure possibly induces charge redistribution from the CuO_2 chain to Cu_2O_3 ladder. Such pressure also transfers the system from a 1D metal to an anisotropic 2D metal, with superconductivity of the ladder occurring in the anisotropic 2D electronic state.

Optical, transport, and NMR measurements suggest a formation of hole pairs associated with pseudogap formation for a high Ca-concentration ($x > 10$) sample at ambient pressure. These hole pairs would be confined within a ladder and unable to hop between ladders. In contrast, charge dynamics along a leg can possibly be characterized by a collective mode of a pinned CDW. Theoretically, both superconductivity and CDW are expected to be ground states in the hole doped two-leg ladder system and may be competing with each other.

In spin gap-mediated superconductivity, while theories predict the d -wave symmetry of the superconducting gap [7], the presence of a coherence peak observed in high- P NMR results seems to rule out simple d -wave superconductivity in $\text{Sr}_{14-x}\text{Ca}_x\text{Cu}_{24}\text{O}_{41}$ [108].

Considering all the research, it is surmised that the superconductivity of $\text{Sr}_{14-x}\text{Ca}_x\text{Cu}_{24}\text{O}_{41}$ probably takes place under the presence of a spin gap, yet the spin gap formation itself does not seem to play a crucial role in superconductivity. At present, the pairing mechanism of $\text{Sr}_{14-x}\text{Ca}_x\text{Cu}_{24}\text{O}_{41}$ remains unclear. Further experimental and theoretical efforts directed at clarifying for example how much the spin gap state contributes and what effect CDW instability applies regarding the pairing mechanism should be useful to elucidate the origin of superconductivity.

Finally, we must emphasize that at this moment $\text{Sr}_{14-x}\text{Ca}_x\text{Cu}_{24}\text{O}_{41}$ is the only spin ladder compound exhibiting superconductivity. It seems a little too naive, however, to conclude that

the experimental results obtained on $\text{Sr}_{14-x}\text{Ca}_x\text{Cu}_{24}\text{O}_{41}$ indeed reflect the general physics of two-leg ladder materials. In fact, $\text{Sr}_{14-x}\text{Ca}_x\text{Cu}_{24}\text{O}_{41}$ cannot be regarded as a simple model case for a two-leg ladder system since the ladder may strongly be influenced by the random potential originating from the large buckling of oxygen atoms in 1D CuO_2 chains. This makes it reasonable to surmise that in order to overcome the excess random potential the superconductivity of $\text{Sr}_{14-x}\text{Ca}_x\text{Cu}_{24}\text{O}_{41}$ shows up not in an “optimal-doped” region but rather in an “over-doped” one. The actual T_c is therefore lower than what should be expected and the relationship between spin gap and superconductivity is not so straightforward. Actually, superconductivity appears at nearly optimal value and clearly decreases with pressure higher than ~ 4.5 GPa. The so-called “under-doped” region observed in high- T_c cuprates where T_c increases toward an optimal value by carrier doping seems to be missing. It is strongly expected that researchers will discover new superconducting ladder materials that are “cleaner” than $\text{Sr}_{14-x}\text{Ca}_x\text{Cu}_{24}\text{O}_{41}$.

ACKNOWLEDGEMENTS

This work was partly supported by a Grant-in-Aid for Scientific Research from the Ministry of Education, Culture, Sports, Science and Technology, Japan.

Two of authors (N. M. and J. A.) are thankful for a Grant-in-Aid for Science Research from the Ministry of Education, Culture, Sports, Science and Technology, Japan and 21st COE program.

REFERENCES

- [1] E. Dagotto, J. Riera and D. Scalapino, *Phys. Rev. B* 45 (1992) 5744.
- [2] T. M. Rice, S. Gopalan and M. Sigrist, *Europhys. Lett.* 23 (1993) 445.
- [3] E. Dagotto and T. M. Rice, *Science* 271 (1996) 618.
- [4] B. Levy, *Phys. Today* (1996) October 17.
- [5] E. Dagotto, *Rep. Prog. Phys.*, 62 (1999) 1525.
- [6] J. G. Bednorz, and K. A. Müller, *Z. Phys.* B64 (1986) 189.
- [7] M. Sigrist, T. M. Rice and F. C. Zhang, *Phys. Rev. B* 49 (1994) 12058
- [8] M. Azuma, Z. Hiroi, M. Takano, K. Ishida and Y. Kitaoka, *Phys. Rev. Lett.*, 73 (1994) 3463.
- [9] Z. Hiroi, M. Azuma, M. Takano and Y. Bando, *J. Solid State. Chem.* 95 (1991) 230
- [10] Z. Hiroi and M. Takano, *Nature* 377 (1995) 41.
- [11] M. Uehara, T. Nagata, J. Akimitsu, H. Takahashi, N. Môri and K. Kinoshita, *J. Phys. Soc. Jpn.* 65 (1996) 2764.
- [12] T. Barnes, E. Dagotto, J. Riera, and E. S. Swanson, *Phys. Rev. B* 47 (1993) 3196.
- [13] S. R. White, R. M. Noack, and D. J. Scalapino, *Phys. Rev. Lett.* 73 (1994) 886.
- [14] Z. Hiroi, *J. Solid State. Chem.* 123 (1996) 223.
- [15] T. Kimura, K. Kuroki and H. Aoki, *Phys. Rev. B* 54 (1996) R9608.
- [16] K. Ishida, Y. Kitaoka, K. Asayama, M. Azuma, Z. Hiroi and M. Takano, *J. Phys. Soc. Jpn.* 63 (1994) 3222.

- [17] K. Kojima, A. Keren, G. M. Luke, B. Nachumi, W. D. Wu, Y. J. Uemura, M. Azuma and M. Takano, Phys. Rev. Lett. 74 (1995) 2812.
- [18] M. Troyer, H. Tsunetsugu, and D. Würtz, Phys. Rev. B 50 (1994) 13515.
- [19] S. Matsumoto, Y. Kitaoka, K. Ishida, K. Asayama, Z. Hiroi, N. Kobayashi and M. Takano, Phys. Rev. B 53 (1996) 11942.
- [20] R. Kadono, H. Okajima, A. Yamashita, K. Ishii, T. Yokoo, J. Akimitsu, N. Kobayashi, Z. Hiroi, M. Takano and K. Nagamine, Phys. Rev. B 54 (1996) 9628.
- [21] E. M. McCarron, M. A. Subramanian, J. C. Calabrese and R. L. Harlow, Mater. Res. Bull 23 (1988) 1355.
- [22] T. Sigrist, L. F. Schneemeyer, S. A. Sunshine, J. V. Waszczak and R. S. Roth, Mater. Res. Bull 23 (1988) 1429.
- [23] R. Eccleston, M. Azuma and M. Takano, Phys. Rev. B 53 (1996) 14721.
- [24] R. Eccleston, M. Uehara, J. Akimitsu, H. Eisaki, N. Motoyama and S. Uchida, Phys. Rev. Lett. 81 (1998) 1702.
- [25] S. Tsuji, K. Kumagai, M. Kato and Y. Koike, J. Phys. Soc. Jpn. 65 (1996) 3474.
- [26] K. Kumagai, S. Tsuji, M. Kato, and Y. Koike, Phys. Rev. Lett. 78, (1997) 1992.
- [27] K. Magishi, S. Matsumoto, Y. Kitaoka, K. Ishida and K. Asayama, M. Uehara, T. Nagata and J. Akimitsu, Phys. Rev. B 57 (1998) 11533.
- [28] L. P. Regnault, A. H. Moudden, J. P. Boucher, E. Lorenzo, A. Hiess, A. Vietkin, A. Revcolevschi, Physica B 259-261 (1999) 1038.
- [29] Y. Mizuno, T. Tohyama, S. Maekawa, T. Osafune, H. Eisaki, and S. Uchida, Phys. Rev. B57 (1998) 5326.
- [30] F. C. Zhang and T. M. Rice, Phys. Rev. B37 (1988) 3759.
- [31] S. A. Carter, B. Batlogg, R. J. Cava, J. J. Krajewski, W. F. Peck Jr. and T. M. Rice, Phys. Rev. Lett. 77 (1996) 1378.
- [32] M. Matsuda, K. Katsumata, T. Yokoo, S. M. Shapiro, and G. Shirane, Phys. Rev. B54 (1996) R15626.
- [33] M. Matsuda, K. M. Kojima, Y. J. Uemura, J. L. Zarestky, K. Nakajima, K. Kakurai, T. Yokoo, S. M. Shapiro, and G. Shirane, Phys. Rev. B57 (1998) 11467.
- [34] M. Kato, K. Shiota and Y. Koike, Physica C 258 (1996) 284.
- [35] M. Matsuda and K. Katsumata, Phys. Rev. B 53 (1996) 12201.
- [36] N. Motoyama, T. Osafune, T. Kakeshita, H. Eisaki, and S. Uchida, Phys. Rev. B55 (1997) R3386.
- [37] M. Matsuda, K. Katsumata, H. Eisaki, N. Motoyama, S. Uchida, S. M. Shapiro, and G. Shirane, Phys. Rev. B54 (1996) 12199.
- [38] L. P. Regnault, J. P. Boucher, H. Moudden, J. E. Lorenzo, A. Hiess, U. Ammerahl, G. Dhalenne, and A. Revcolevschi, Phys. Rev. B59 (1999) 1055.
- [39] M. Matsuda, T. Yosihama, K. Kakurai, and G. Shirane, Phys. Rev. B59 (1999) 1060.
- [40] M. Takigawa, N. Motoyama, H. Eisaki and S. Uchida, Phys. Rev. B57 (1998) 1124.
- [41] T. Imai, K. R. Thurber, K. M. Shen, A. W. Hunt and F. C. Chou, Phys. Rev. Lett., 81 (1999) 220.
- [42] Z. Hiroi, S. Amelinckx, G. Van Tendeloo, and N. Kobayashi, Phys. Rev. B 54 (1996) 15849.
- [43] D. E. Cox, T. Iglesias, K. Hirota, G. Shirane, M. Matsuda, N. Motoyama, H. Eisaki, and S. Uchida, Phys. Rev. B57 (1998) 10750.
- [44] T. Fukuda, J. Mizuki, and M. Matsuda, Phys. Rev. B66 (2002) 12104.

- [45] Y. Gotoh, I. Yamaguchi, Y. Takahashi, J. Akimoto, M. Goto, M. Onoda, H. Fujino, T. Nagata and J. Akimitsu, Phys. Rev. B 68 (2003) 224108.
- [46] S. van Smaalen, Phys. Rev. B67 (2003) 26101.
- [47] M. Kato, T. Adachi, and Y. Koike, Physica C265 (1996) 107.
- [48] M. Matsuda, K. Katsumata, H. Eisaki, N. Motoyama, S. Uchida, T. Yokoo, S. M. Shapiro, G. Shirane, and J. L. Zarestky, Phys. Rev. B56 (1997) 14499.
- [49] T. Osafune, N. Motoyama, H. Eisaki and S. Uchida, Phys. Rev. Lett., 78 (1997) 1980.
- [50] U. Ammerahl, B. Büchner, C. Kerpen, R. Gross, and A. Revcolevschi, Phys. Rev. B62 (2001) 2882.
- [51] V. Kataev, K.-Y. Choi, M. Grüninger, U. Ammerahl, B. Büchner, A. Freimuth, and A. Revcolevschi, Phys. Rev. Lett. 86 (2001) 2882.
- [52] V. Y. Yushankhai and R. Hayn, Europhys. Lett. 47 (1999) 116.
- [53] S. Tornow, O. Entin-Wohlman, and A. Aharony, Phys. Rev. B60 (1999) 10206.
- [54] M. Matsuda, K. Kakurai, J.-E. Lorenzo, L.-P. Regnault, A. Hiess, and G. Shirane, Phys. Rev. B68 (2003) R060406.
- [55] R. Leidl and W. Selke, Phys. Rev. B69 (2004) 56401.
- [56] W. Selke, V. L. Pokrovsky, B. Büchner, and T. Kroll, Eur. Phys. J. B30 (2002) 83.
- [57] M. Holtschneider and W. Selke, Phys. Rev. E68 (2003) 26120.
- [58] R. Weht, W. E. Pickett, Phys. Rev. Lett. 81 (1998) 2502.
- [59] M. Matsuda, K. Kakurai, H. Yamaguchi, T. Ito, C. H. Lee, and K. Oka, Applied Physics A74 (2002) S637.
- [60] U. Staub, B. Roessli, A. Amato, Physica B289-290 (2000) 299.
- [61] E. M. L. Chung, G. J. McIntyre, D. McK. Paul, G. Balakrishnan, and M. R. Lees, Phys. Rev. B68 (2003) 144410.
- [62] P. K. Davis, J. Solid State Chem. 95 (1991) 365.
- [63] P. K. Davis, E. Caignol, and T. King, J. Am. Ceram. Soc. 74 (1991) 569.
- [64] A. Hayashi, B. Batlogg, and R. J. Cava, Phys. Rev. B58 (1998) 2678.
- [65] M. Matsuda, K. Ohyama, and M. Ohashi, J. Phys. Soc. Jpn. 68 (1999) 269.
- [66] H. F. Fong, B. Keimer, J. W. Lynn, A. Hayashi, and R. J. Cava, Phys. Rev. B59 (1999) 6873.
- [67] K. Kudo, S. Kurogi, Y. Koike, T. Nishizaki, and N. Kobayashi, cond-mat/0408628.
- [68] M. D. Chabot and J. T. Markert, Phys. Rev. Lett. 86 (2001) 163.
- [69] S. Kurogi, K. Kudo, T. Noji, Y. Koike, T. Nishizaki, and N. Kobayashi, J. Low Temp. Phys. 131 (2003) 353.
- [70] J. Dolinsek, D. Arcon, P. Cevc, O. Milat, M. Miljak, and I. Aviani, Phys. Rev. B57 (1998) 7798.
- [71] Z. Hiroi, M. Okumura, T. Yamada, and M. Takano, J. Phys. Soc. Jpn. 69 (2000) 1824.
- [72] M. Isobe, K. Kimoto, and E. Takayama-Muromachi, J. Phys. Soc. Jpn. 71 (2002) 782.
- [73] Y. Mizuno, T. Tohyama, and S. Maekawa, Phys. Rev. B60 (1999) 6230.
- [74] M. Matsuda, H. Yamaguchi, T. Ito, C. H. Lee, K. Oka, Y. Mizuno, T. Tohyama, S. Maekawa, and K. Kakurai, Phys. Rev. B63 (2001) 180403(R).
- [75] S. K. Satija, J. D. Axe, R. Gaura, R. Willett, and C. P. Landee, Phys. Rev. B25 (1982) 6855.
- [76] M. Matsuda, K. Kakurai, S. Kurogi, K. Kudo, Y. Koike, H. Yamaguchi, T. Ito, and K. Oka, in preparation.
- [77] H. Yamane, Y. Miyazaki and H. Hirai, J. Ceramic Soc. Jpn., 98 (1990) 105.

- [78] M. Matsuda, K. Katsumata, R. S. Eccleston, S. Brehmer, and H. J. Mikeska, *Phys. Rev. B* 62 (2000) 8903.
- [79] S. Sugai and M. Suzuki, *Phys. Stat. Sol. (b)*, 215 (1999) 653.
- [80] A. Gozar, G. Blumberg, B. S. Dennis, B. S. Shastry, N. Motoyama, H. Eisaki, and S. Uchida, *Phys. Rev. Lett.* 87 (2001) 197202.
- [81] S. Katano, T. Nagata, J. Akimitsu, M. Nishi and K. Kakurai, *Phys. Rev. Lett.*, 82 (1999) 636.
- [82] S. Fujiyama, M. Takigawa, N. Motoyama, H. Eisaki and S. Uchida, *J. Phys. Soc. Jpn.* 69 (2000) 1610.
- [83] T. Nagata, H. Fujino, J. Akimitsu, M. Nishi, K. Kakurai, S. Katano, M. Hiroi, M. Sera, and N. Kobayashi, *J. Phys. Soc. Jpn.*, 68 (1999) 2206.
- [84] S. Ohsugi, M. Magishi, S. Matsumoto, Y. Kitaoka, T. Nagata and J. Akimitsu, *Phys. Rev. Lett.*, 82 (1999) 4715.
- [85] M. Isobe, Y. Uchida and E. Takayama-Muromachi, *Phys. Rev. B* 59 (1999) 8703.
- [86] K. Ohishi, T. Yokoo, K. Kakuta, H. Fujino, T. Nagata, J. Akimitsu and R. Kadono, *J. Phys. Soc. Jpn.*, 69 (2000) 2427.
- [87] T. Nagata, H. Fujino, K. Satoh, N. Yamamori, J. Akimitsu, S. Katano, M. Nishi, K. Kakurai, M. Hiroi, M. Sera, and N. Kobayashi, K. Tenya, H. Amitsuka, T. Takigawa, H. Inago and T. Sakakibara, *J. Phys. Soc. Jpn.*, 68 (1999) 2206.
- [88] M. Isobe, M. Onoda, T. Ohta, F. Izumi, K. Kimoto, E. Takayama-Muromachi, A. W. Hewat, and K. Ohoyama, *Phys. Rev. B* 62 (2000) 11667.
- [89] K. M. Kojima, N. Motoyama, H. Eisaki and S. Uchida, *J. Electron Spectroscopy and Related Phenomena* 117-118 (2001) 237.
- [90] T. Takahashi, T. Yokoya, A. Ashihara, H. Fujisawa, A. Chainani, M. Uehara, T. Nagata, J. Akimitsu and H. Tsunetsugu, *Phys. Rev. B* 56 (1997) 7870.
- [91] N. Nücker, M. Merz, C. A. Kuntscher, S. Gerhold, S. Schuppler, R. Neudert, M. S. Golden, J. Fink, D. Schild, S. Stadler, V. Chakarian, J. Freeland, Y. U. Idzerda, K. Conder, M. Uehara, T. Nagata, J. Goto, J. Akimitsu, N. Motoyama, H. Eisaki, S. Uchida, U. Ammerahl, and A. Revcolevschi, *Phys. Rev. B* 62 (2000) 14384.
- [92] T. Timusk and B. Statt, *Rep. Prog. Phys.*, 62 (1999) 61.
- [93] T. Osafune, N. Motoyama, H. Eisaki, S. Uchida, and S. Tajima, *Phys. Rev. Lett.*, 82 (1999) 1313.
- [94] B. Ruzicka, L. Degiorgi, U. Ammerahl, G. Dhalenne and A. Revcolevschi, *Eur. Phys. J. B* 6 (1998) 301
- [95] H. Kitano, R. Inoue, T. Hanaguri, A. Maeda, N. Motoyama, M. Takaba, K. Kojima, H. Eisaki and S. Uchida, *Europhys. Lett.* 56 (2001) 434. ; *Physica C* 341-348, (2000) 463.
- [96] A. Maeda, R. Inoue, H. Kitano, N. Motoyama, H. Eisaki, and S. Uchida, *Phys. Rev. B* 67 (2003) 115115.
- [97] B. Gorshunov, P. Haas, T. Rößm, M. Dressel, T. Vuletić, B. Korin-Hamzić, S. Tomić, J. Akimitsu and T. Nagata, *Phys. Rev. Lett.*, 66 (2002) 060508.
- [98] T. Vuletić, B. Korin-Hamzić, S. Tomić, B. Gorshunov, P. Haas, T. Rößm, M. Dressel, J. Akimitsu, T. Sasaki and T. Nagata, *Phys. Rev. Lett.*, 90 (2003) 2570021.
- [99] G. Blumberg, P. Littlewood, A. Gozar, B. S. Dennis, N. Motoyama, H. Eisaki, and S. Uchida, *Science* 297 (2002) 584.
- [100] C. Hess, H. ElHaes, B. Büchner, U. Ammerahl, M. Hücker, and A. Revcolevschi, *Phys. Rev. Lett.* 93 (2004) 027005.

- [101] K. Kudo, S. Ishikawa, T. Noji, T. Adachi, Y. Koike, K. Maki, S. Tsuji and K. Kumagai, *J. Phys. Soc. Jpn.*, 70 (2001) 437.
- [102] M. Uehara, M. Ogawa and J. Akimitsu, *Physica C* 255 (1995) 193.
- [103] M. Isobe, T. Ohta, M. Onoda, F. Izumi, S. Nakano, J. Q. Li, Y. Matsui, E. Takayama-Muromachi, T. Matsumoto and H. Hayakawa, *Phys. Rev. B* 57 (1998) 613.
- [104] T. Ohta, F. Izumi, M. Onoda, M. Isobe, E. Takayama-Muromachi and A. W. Hewat, *J. Phys. Soc. Jpn.*, 66 (1997) 3107.
- [105] H. Mayaffre, P. Auban-Senzier, M. Nardone, D. Jérôme, D. Poilblanc, C. Bourbonnais, U. Ammerahl, G. Dhalenne and A. Revcolevschi, *Science* 279 (1998) 345.
- [106] Y. Piskunov, D. Jerome, P. Auban-Senzier, P. Wzietek, Y. Ammerhal, G. Dhalenne and A. Revcolevschi, *Eur. Phys. J. B* 13 (2000) 417.
- [107] Y. Piskunov, D. Jerome, P. Auban-Senzier, P. Wzietek, C. Bourbonnais, U. Ammerhal, G. Dhalenne and A. Revcolevschi, *Eur. Phys. J. B* 24 (2001) 443.
- [108] N. Fujiwara, N. Môri, Y. Uwatoko, T. Matsumoto, N. Motoyama and S. Uchida, *Phys. Rev. Lett.*, 90 (2003) 1370011.
- [109] H. Tsunetsugu, M. Troyer and T. M. Rice, *Phys. Rev. B* 49 (1994) 16078.
- [110] T. Nagata, M. Uehara, J. Goto, J. Akimitsu, N. Motoyama, H. Eisaki, S. Uchida, H. Takahashi, T. Nakanishi, and N. Môri, *Phys. Rev. Lett.*, 81 (1998) 1090.
- [111] Y. Fukuzumi, K. Mizuhashi, K. Takenaka and S. Uchida, *Phys. Rev. Lett.*, 76 (1996) 684.
- [112] N. Motoyama H. Eisaki, S. Uchida, N. Takeshita, N. Môri, T. Nakanishi and H. Takahashi, *Europhysics Letters* 58 (2002) 758.
- [113] T. Nakanishi, H. Takahashi, N. Takeshita, N. Môri, N. Motoyama, H. Eisaki, S. Uchida, H. Fujino, T. Nagata and J. Akimitsu, *Physica B* 281&282 (2000) 957.